



Estimating Gross and Net Primary Productivities Using Earth Observation Products: a Review

Hamed Sabzchi-Dehkharghani¹ · Asim Biswas² · Sarita Gajbhiye Meshram³ · Abolfazl Majnooni-Heris¹

Received: 15 November 2022 / Accepted: 24 August 2023 / Published online: 3 October 2023
© The Author(s), under exclusive licence to Springer Nature Switzerland AG 2023

Abstract

Considerable research has been conducted on the estimation of Gross Primary Productivity (GPP) and Net Primary Productivity (NPP) from different viewpoints. Each vision has proposed special applied materials and methodologies and has provided specific insight into the results and overall conclusions. As NPP generally declines once crops start to begin competing intensively for water resources, the identification of precise NPP estimation approaches can be of importance in water and agricultural studies. Due to the lack of a comprehensive overview of the subject that investigates GPP and NPP studies from both environmental and agricultural perspectives, we reviewed the existing approaches in estimating these two parameters with a special focus on estimating NPP for agricultural studies. Categorization of the diverse proposed models and approaches, with special attention to the role of newly introduced materials, such as chlorophyll proxies, is provided on GPP and NPP estimations. After introducing the different categories, from the environmental perspective, we addressed the most recent improvements in GPP estimations in the biosphere by applying a chlorophyll-based fraction of Absorbed Photosynthetically Active Radiation (fPAR) into the light use efficiency (LUE) model. Then, by considering the agricultural perspectives, the application of both chlorophyll-based fPAR and a new chlorophyll-based predictor was discussed to estimate NPP and yield. It is expected that the outlined vision on estimating NPP in agricultural studies helps to identify the current boundary of knowledge in these types of studies.

Keywords Environmental monitoring · Gross Primary Productivity · Net Primary Productivity · Chlorophyll proxies

1 Introduction

A portion of the radiated energy to the canopy is stored by the process of photosynthesis in organic substances; this is known as Gross Primary Productivity (GPP). The other portion is either re-radiated or lost as latent heat [1]. GPP and its derivatives have been the focus of various terrestrial sciences, and it is a common term in interdisciplinary research. In hydrology, there have been attempts at quantifying the available root zone soil moisture sink according to the connection between evapotranspiration (ET) and Leaf Area

Index (LAI). Since LAI is a proxy for the anatomized portion of the GPP in ecology, it connects GPP to soil moisture in ecohydrology [2–7]. Not all GPP incarnates into the Net Primary Productivity (NPP) since a part of it is consumed for the plant autotrophic respiration (R_a) process through which the plant respire carbon for growth (R_G) and maintenance (R_M) [8]. Each major organ of a plant (leaf, stem, and root) respire carbon for its growth and maintenance. This can be studied in the combined field of ecological and plant phenological sciences to connect the concepts of GPP and NPP [9–11]. Subtracting R_a from GPP, the first derivative of GPP will be calculated as NPP which is measured for estimating the rate of biomass accumulation [12]. NPP represents the net C uptake from the atmosphere into vegetation [12] and can be calculated as the sum of biomass increment, mortality, and turnover of foliage and fine roots [13]. The total biomass can be transformed into crop yield in farmlands using the Harvest Index (HI) if the index is multiplied by the accumulated amount of biomass during the crop growing period [14–16].

✉ Abolfazl Majnooni-Heris
majnooni@tabrizu.ac.ir

¹ Department of Water Engineering, Faculty of Agriculture, University of Tabriz, Tabriz 51666-16471, Iran

² School of Environmental Sciences, University of Guelph, Guelph, Canada

³ WRAM Research Lab Pvt., Ltd, Nagpur 440027, Maharashtra, India

NPP, biomass, and yield are estimated in agricultural studies while they are still connected to ecohydrology and biology through GPP and R_a [17]. Heterotrophic respiration (R_h) is the total flux of carbon to the biosphere caused by the decomposition process (R_D) and by the respiration of non-plant organisms (R_O) [18]. Both R_a and R_h estimations are within the fields of ecology, biogeochemistry, and dynamic biogeography sciences; these can be subtracted from GPP to produce the second derivative of GPP known as net ecosystem exchange (NEE). NEE can be directly monitored by site level measurements through the global eddy covariance (EC) tower network [19–21]. GPP can be calculated indirectly by in situ measured NEE values that can be extrapolated to the gridded global NEE values using earth observation data [22]. GPP is calculated indirectly because it is impossible to directly observe daytime GPP or ecosystem respiration, and that is why it is typically inferred from measurements of NEE [23]. Recently, solar-induced chlorophyll fluorescence (SIF) has been shown to be well correlated to GPP, thus offering a path to improve the NEE partitioning by constraining GPP [24].

GPP can also be estimated at global scale using the models that connect soil, vegetation, and atmosphere parameters. These connections are reflected in conceptualizing soil, vegetation, and atmosphere dynamic models for the biosphere that capture the effect of water loss, water stress, nutrition, and age on the stomatal operation and the subsequent amount of LAI. Examples of these models are soil-vegetation-atmosphere transfer (SVAT), dynamic global vegetation model (DGVM) and ORganizing Carbon and Hydrology In Dynamic Ecosystem (ORCHIDEE) [25–30]. In these models, LAI is one of the determiners for ET, in addition to other predictors, such as precipitation, runoff, infiltration, soil texture, and topography because LAI can be connected to the available moisture in the root zone by ET. Instead of estimating terrestrial GPP using multiparameter models, the estimation process can be simplified using an ecological concept called the efficiency model (PEM) or the light use efficiency (LUE) model [31]. Despite the apparent simplicity of the LUE model that estimates GPP by multiplying three terms, the photosynthetically active radiation (PAR), the fraction of absorbed PAR (fPAR), and the LUE factor, however, fPAR and LUE factors are controversial. LUE is often calculated as a function of maximum daily LUE (ϵ_{\max}) regulated by environmental controls (temperature, soil water, vapor pressure deficit, etc.) [32–34]. Traditionally, the whole canopy proxies were used to define fPAR and LUE, while recently, the controversy behind the fPAR and LUE definitions refers to the assumption that the absorption of PAR by the canopy's chlorophyll part is effective in producing GPP rather than the absorption by the whole canopy [35]. Solar-induced fluorescence (SIF) is the proxy of chlorophyll content which can be sensed remotely and has great potential

for estimating GPP due to a strong observed relationship between them from both ground-based and satellite observations [36]. From the environmental perspective, the importance of the in situ NEE measurements and subsequent GPP calculation using complicated dynamic or LUE models is to understand the role of carbon in the global climate system. Hence, GPP and its derivatives have been studied to investigate the process of carbon sequestration and release, feedback between climate and vegetation change, heat, momentum, and moisture fluxes as well as global greenhouse gas concentrations [37–40].

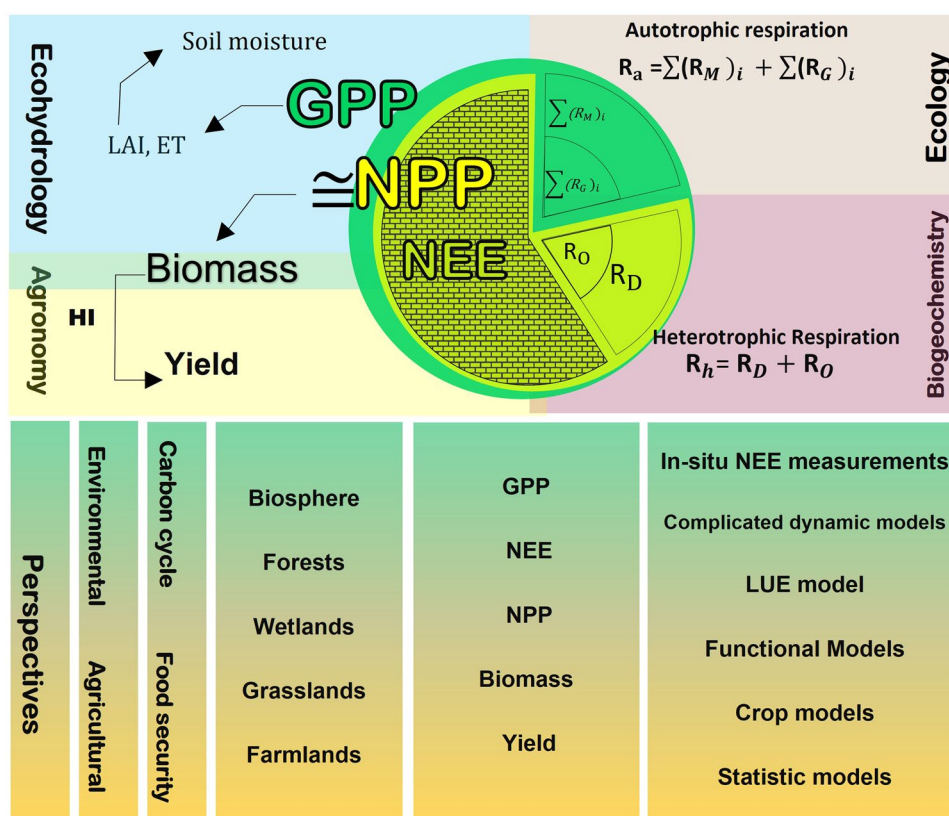
GPP and NPP estimations also exist in regional-scaled studies on ecosystem preservation, reclamation, and production in wetlands, grasslands, and farmlands [41–44]. From the agricultural perspective, data on the accumulated amount of biomass during the early growing stage until harvest time is important to meet the information demand for food security planners and policymakers [45–47]. Spatiotemporal distribution of NPP and biomass on farmlands can help scientists to determine the potential and scope of improvements on agricultural lands for predicting yield values before harvest and for providing early warnings to traders, farmers, and insurance companies [48, 49]. Different approaches for regional estimation of GPP and NPP can be classified into three main categories: mechanistic, statistical, and functional [48]. Mechanistic models are usually known as crop models based on the dominant physical and biophysical principles in a system consisting of crop, soil, and atmosphere. If there is enough detailed information from plant peripherals, litter circumstances, and agricultural managing inputs and in integration with assimilated remote sensing (soil moisture and LAI) data, crop models can provide an acceptable estimation of NPP [50–52]. When there is a lack of detailed information, statistic and functional models are used to make assumptions on the relationship among the existing field-measured predictors and NPP or to identify the best combination of predictors that contribute the most variance to NPP. Functional models are indeed simplified versions of the complex mechanistic models in combination with statistical schemes [53–55]. After modeling and identification of effective predictors, the monitored values of these predictors are imported into forecasting methods to estimate future crop yield and produce early warnings [48, 56]. In classical forecasting approaches, an attempt is made to differentiate seasonality and trend components of the predictors' time series, and then by assuming that these discovered trends are constant, the forecast is made for the target parameter, while in newly developed approaches, models are updated each time for new observation [57–59]. However, required information about weather, soil properties, and precise land cover data to build a ground-data-dependent functional model are typically not available in developing countries, where reliable

yield predictions are most needed [54]. In this case, machine learning ideas like deep learning architectures by which the model automatically learns useful features only from multi-spectral remote sensing images seem to be the only solution for making crop yield predictions. In an attempt, remotely sensed multispectral images have been used in the deep long short-term memory (LSTM architecture to estimate and forecast crop yield [60].

Inferred from the previous explanations, Fig. 1 shows the contribution of different fields of knowledge in studying GPP and its derivatives and indicates their estimation approaches in environmental and agricultural perspectives. As shown in Fig. 1, ecohydrological investigations with environmental perspective require the consideration of several crucial parameters (such as GPP, ET, LAI, and soil moisture) to the understanding of the complex interactions between ecological and hydrological processes within a biosphere. While in ecology and biochemistry the attempt is to understand respiration processes, they are used to generate NPP and NEE derivatives from GPP. The figure also depicts that the environmental perspective aims to monitor carbon cycle in the biosphere including forest and wetland land use. On the other hand, the agricultural perspective aims to study food security in grassland and farmland land use. While GPP and its first-hand derivatives are the target parameters in environmental studies, the latest derivatives

of it like biomass and yield are the specific targets of interest for agricultural studies. In environmental studies, in situ NEE measurements are used for conducting direct estimations or for validating the dynamic models, while the LUE model is used for reducing the complicity of the estimation process instead of dynamic models. Conversely, within the realm of agricultural studies, the utilization of crop models, statistical models, and newly developed functional models that leverage remote sensing data has facilitated the research process pertaining to agricultural lands. These models prove particularly valuable in cases where the measured biomass or yield serves as the validation indicator. In this paper, after a review on the use of global models from the environmental perspective in the "Introduction" section, the rest of the paper focus on the application of the LUE and functional models from the agricultural perspective. Figure 2 shows the relationship between the main terms reviewed and their proximity to environmental and agricultural perspectives, and Table 1 describes the contents clarified in each paragraph or subsection and their interconnections. Here, with a special emphasis on the most recent improvements in terrestrial GPP estimations using chlorophyll-based fPAR and LUE concepts, the importance of future studies on the application of chlorophyll-based predictors in functional models became apparent. From the agricultural perspective, an argue on the regional application of chlorophyll-based fPAR

Fig. 1 Contribution of different fields of knowledge in studying GPP and its derivatives outlined into the two environmental and agricultural perspectives



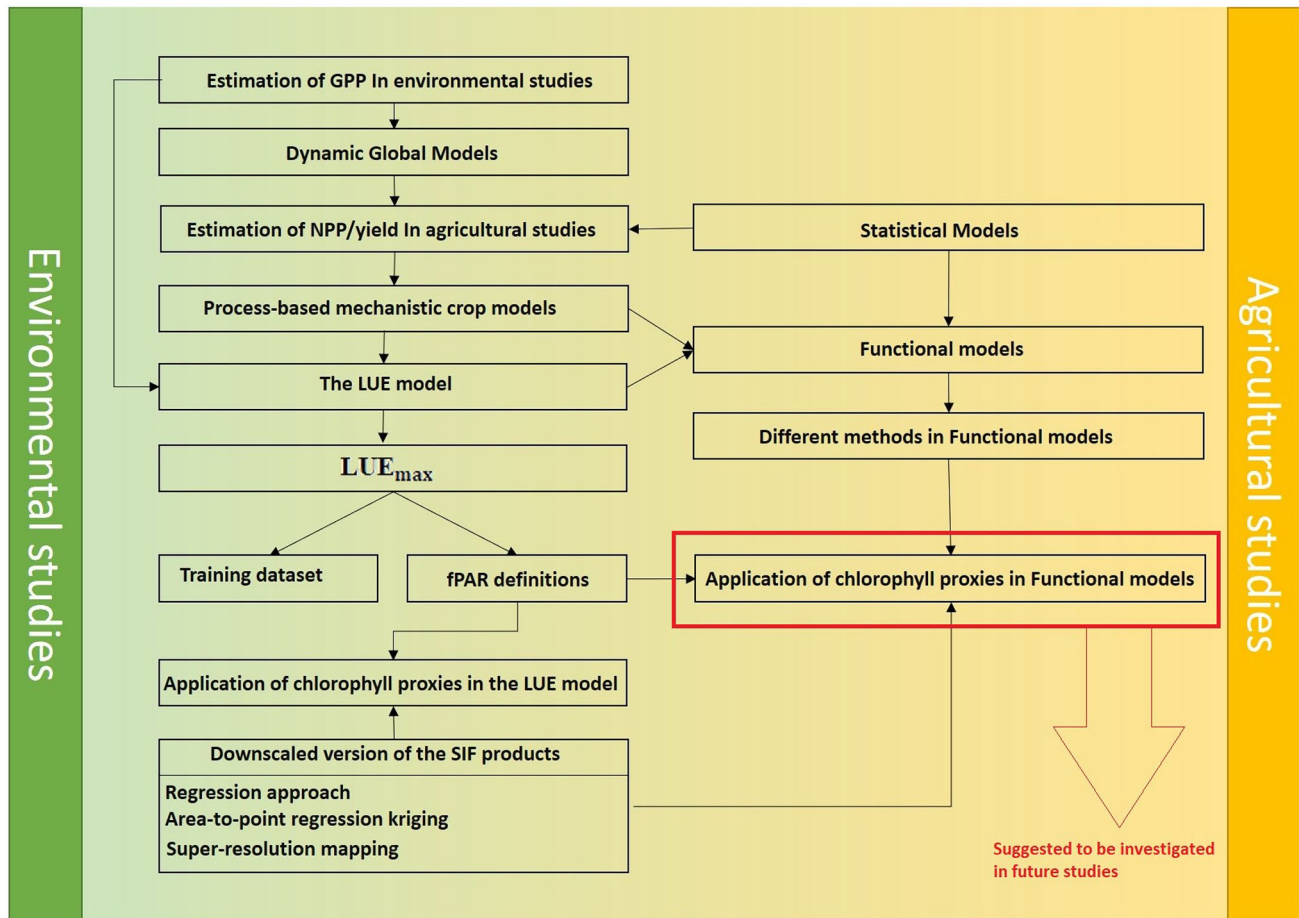


Fig. 2 The relationship between the main reviewed terms and their proximity to environmental and agricultural perspectives

on the LUE model was raised and recommended to be tested in future studies using downscaled version of remote sensing chlorophyll products. At the end, a new chlorophyll-based remote sensing predictor was introduced for being tested in functional models in estimating NPP.

2 Crop Models

Crop models are categorized into mechanistic model classes that can be used to model the crop growth duration and NPP for agricultural purposes [61, 62]. A crop model simulates crop growth based on information about the crop litter and surrounding atmosphere, furthermore, it can be used to build a comprehensive dynamic biosphere model if it is integrated with a climate change model. A crop model also can be embedded in a hydrological model to explain the interactions between the crop and the hydrological circumstances around it [63–65]. Many crop models have been developed for each major agricultural crop such as wheat, maize, and rice in different parts of the world [66–69]. Equations that

include explanatory variables and parameters in relation to CO_2 , solar radiation, temperature, humidity, wind speed, precipitation, available water, and nutrients provide crop models to determine the required state variables [70]. In some of these models, a linear or a nonlinear temperature response function with an upper limit for the developmental rate is considered to simulate crop growth, while other models consider a function with an optimum temperature above which the growth rate decreases with the temperature increase [71, 72]. Among the crop models, those assume that NPP is driven by the amount of solar radiation and CO_2 and is moderated by temperature use different concepts such as canopy light use efficiency model, single-leaf photosynthesis light-response model, and Farquhar-von Caemmerer-Berry biochemical model [31, 73, 74]. Because not all model parameters can be determined directly by measuring explanatory variables, a crop model needs to be carefully calibrated, including from the lowest calibration level only containing end-season agronomic measurements to the highest level containing both in-season and end-season measurements based on the calibration goals. By fitting the overall

Table 1 Contents clarified in each paragraph or subsection and their interconnections

Section	Paragraph/subsection	Summary of the paragraph/subsection	Connection to the next section
1. Introduction	Paragraph 1	<ul style="list-style-type: none"> ✓ Defines GPP and its derivatives after plant autotrophic and heterotrophic respiration (respirations were also described in this paragraph) ✓ Describes why GPP and its derivatives are considered in various terrestrial sciences: <ul style="list-style-type: none"> • To investigate different types of plant and organisms' respirations in ecology • To quantify the available root zone soil moisture, sink in ecohydrology • To estimate the rate of biomass accumulation (the net carbon uptake from the atmosphere into vegetation) in agronomy ✓ Describes how to measure GPP 	After getting introduced with GPP and its derivatives, the next paragraph reviews how GPP can be estimated at global scale
	Paragraph 2	<ul style="list-style-type: none"> ✓ Describes the concept of soil, vegetation, and atmosphere dynamic models for the biosphere that are used to model and estimate GPP ✓ Describes an alternative concept called the efficiency model (PEM) or the light use efficiency (LUE) model used for estimating GPP instead of multiparameter models ✓ Describes a traditional approach that uses the whole canopy proxies to define the LUE model parameters ✓ Describes a new approach in defining the LUE model parameters in which the fundamental assumption is that only the canopy's chlorophyll part is effective in producing GPP 	After getting introduced with GPP estimating models that works at global scale, the subsequent paragraph highlights the significance of regional estimates for GPP and NPP and outlines various methods for estimating them on areal scale. The application of functional models that work with remote sensing data is bolded in the next paragraph
	Paragraph 3	<ul style="list-style-type: none"> ✓ Highlights GPP and NPP estimation in regional scale including in agricultural studies ✓ Mentions the role of estimating spatiotemporal distribution of NPP and biomass on farmlands ✓ Describes the different approaches for regional estimation of GPP and NPP in three main categories—mechanistic, statistical, and functional: <ul style="list-style-type: none"> • Describes the application and requirements of the crop models • Describes the application and requirements of the functional models • Describes the application of the machine learning models that use multispectral images as the only input data 	After getting introduced with GPP and NPP estimating models that works at regional scale, the next paragraph depicts the flow of the topics presented in the manuscript. It also depicts the area of focus in the present review

Table 1 (continued)

Section	Paragraph/subsection	Summary of the paragraph/subsection	Connection to the next section
	Paragraph 4	<ul style="list-style-type: none"> ✓ By inferring from paragraphs 1, 2, and 3, it depicts connections among different field of knowledge that investigate GPP and its derivatives ✓ Explains that the rest of the review is mostly from the agricultural perspective and focus on the application of the LUE and functional models for agricultural purposes ✓ Shows the flow of the presented topics in this review ✓ Shows that the emphasis is on most recent improvements in the LUE model with chlorophyll proxies and the attempt is to spread the concept it into functional models 	After depicting the flow of the presented topics, the next section starts to review the application of crop models in estimating NPP for agricultural purposes
2. Crop models	Paragraph 1	<ul style="list-style-type: none"> ✓ Describes the application of crop models and their restrictions due to dependency on the enormous number of explanatory variables ✓ Describes different assumptions for the response function of the crop models and the necessity to a careful calibration procedure before application 	Following a detailed exposition of the parameters and algorithms utilized by crop models to estimate NPP, the present section provides a logic for considering the LUE model in related studies by elaborating the limitations of the crop models. The provided logic leads the next paragraph to review the LUE model
	Paragraph 2	<ul style="list-style-type: none"> ✓ Describes other differences between crop models that cause large uncertainty in crop yield simulations ✓ Describes under which circumstance crop models can be used to generate gridded estimations of NPP ✓ Describes the advantage of the LUE model in simplifying the complex processes of plant photosynthesis and respiration compared to crop models 	
3. The LUE model	Paragraph 1	<ul style="list-style-type: none"> ✓ Introduces the application of the LUE model, its parameters, and regulators <p>Explains why a rigorous parameterization and calibration process are required in developing the ✓ LUE model and how it may affect the estimation of net amount of solar energy stored by photosynthesis</p> <ul style="list-style-type: none"> ✓ Describes how the differences in the data used in calibration process and the concepts through which fPAR was defined resulted in a discrepancy in the reported LUE values 	After describing the inherent differences in the studies that used the LUE model, the sources from which these differences arise (calibration data and fPAR definition concepts) are reviewed in detail in the next subsections

Table 1 (continued)

Section	Paragraph/subsection	Summary of the paragraph/subsection	Connection to the next section
Paragraph 2 (LUE _{E_{max}} based on training dataset)	<p>Describes that any change in the left-hand side of the LUE equation (any desired target parameter which can be GPP, NPP, or dry material) enquires correspondent measured dataset for calibrating the model and reinterpreting LUE_{E_{max}}</p>	<p>After describing various concepts related to defining predictor parameters for the LUE model, the subsequent section explains the utilization of remote sensing chlorophyll proxies in the LUE model</p>	
Paragraph 3 (LUE _{E_{max}} based on the fPAR definitions)	<ul style="list-style-type: none"> ✓ Describes different concepts in the definition of fPAR based on accounting or eliminating the intercepted part of the incoming radiation by the non-photosynthetic organs in estimating GPP and its derivatives. These concepts lead to different interpretations of the parameters of the LUE model ✓ Describes how consideration of only the photosynthetic part change the concept of PAR_{Canopy} to PAR_{Chl} and how the concept benefit from remote sensing chlorophyll proxies in the modeling process 		
Paragraph 4 (Application of chlorophyll proxies in the LUE model)	<ul style="list-style-type: none"> ✓ Describes and categorizes available remote sensing chlorophyll proxies (since 2007) into two SIF and chlorophyll index products ✓ Describes the limitation of SIF products that prevents their application for agricultural purposes due to their coarse spatial resolution ✓ Suggests that new high-resolution SIF products or advanced downscaling techniques may increase their contribution to estimating NPP, biomass, and yield estimations on farmlands ✓ Generates a form of the LUE model that works with PAR_{Chl} and LUE_{E_{max}} concepts 	<p>After suggesting the application of downscaled SIF products in the LUE model (since the original version of SIF products specially before 2016 are too coarse for agricultural studies), the next four subsections review some of the downscaling methods that can be used to generate high-resolution SIF products</p>	
SubSects. 3.4.1 to 3.4.3 (Downscaled version of the SIF products)	<ul style="list-style-type: none"> ✓ Describes four downscaling techniques applicable on SIF products including regression approach, area-to-point regression kriging, super-resolution mapping, and long-term temporally corrected and spatially downscaled SIF product 	<p>After investigating the feasibility of access to downscaled version of the SIF products, in the next sections, application of these products in the functional models is discussed. But at first, a review on the functional models themselves is provided</p>	

Table 1 (continued)

Section	Paragraph/subsection	Summary of the paragraph/subsection	Connection to the next section
4. Functional models	Paragraph 1	<ul style="list-style-type: none"> ✓ Describes the functional models as the simplified versions of the complex mechanistic models that estimate crop yield utilizing approximate equations and remote sensing data ✓ Describes the contribution of statistical and mechanistic equations and remote sensing data in building a functional model 	After describing the utilized frameworks for building functional models with the aim of estimating crop yield in agricultural studies, the next subsection suggests application of chlorophyll proxies is in functional models
	SubSects. 4.1 (Different methods in functional models)	Describes two different utilized approaches in building functional models in the literature. One of these approaches based on an empirical equation between fPAR and LAI. The other approach converts LAI values obtained from a crop model to pseudo-vegetation index observations using empirical equations	
	SubSects. 4.2 (Application of chlorophyll proxies in functional models)	<ul style="list-style-type: none"> ✓ Suggests the test of chlorophyll proxies in functional models for future studies with the aim of estimating NPP and yield for agricultural purposes, based on the reviewed promising results from the use of these proxies in estimating GPP using LUE models ✓ Introduces a new chlorophyll-based predictor for being tested in the proposed structures of functional models (a single linear regression and a multiple linear models) with the aim of estimating NPP and yield. Regarding the nonlinearity of the relationship between SIF and GPP, it recommends bringing the nonlinear functions or non-constant coefficients into tests for future studies 	This subsection reaches the main goal of the review paper in which chlorophyll proxies are suggested for being tested in functional studies in the future studies
	Conclusion		

model to a portion of the observed data and then critically validating the model by using the remainder of the observed data, the robustness of the models across environments can be assessed [75]. After the calibration and validation processes, it is possible to analyze the response of a crop in different scenarios by replacing the measured values with scenario-based values for different variables [70, 76].

Crop models vary in terms of the way they involve variables in growth simulation. They simulate the effect of temperature on the rate of crop development [77] and on spikelet fertility [78, 79] in addition to their different CO_2 -fixation algorithms that lead to various responses to climate change factors [80]. Studies have investigated the single-leaf photosynthesis response to the amount of light and the biochemical responses of the plant depending on the amount of CO_2 concentration to determine how the effect of CO_2 should be incorporated into the crop models [81, 82]. Crop models cannot solely be used to generate spatial distribution of NPP. Integration of crop models into the Geographic Information System (GIS)-based Environmental Policy Integrated Climate (GEPIC) (including six types of input data: DEM, soil map, land use map, climate data, plant data, and management data such as irrigation and fertilizer) simulates the effect of elevation on crop dynamics and provides gridded estimations of NPP [83, 84]. Taking advantage of DEM, a semi-distributed hydrological model like Soil and Water Assessment Tool (SWAT) configures sub-basins to connect embedded crop modelers and hydrologic analyzer systems together for estimating the distribution of NPP and biomass on farmlands [85, 86]. Embedded crop modelers of SWAT can also be used for environmental purposes like for estimating NPP in the forest ecosystems by adjusting SWAT default parameters for this type of ecosystems [87]. Process-based mechanistic crop models are effective means to estimate NPP and crop yield, however, these models create large uncertainty in simulations [88]. Application of the LUE model in estimating crop NPP instead of a mechanistic crop model can simplify the complex physiological, biophysical, and biogeochemical processes of plant photosynthesis and respiration [89].

3 The LUE Model

In addition to its application as a crop model, the simplicity of the LUE model has made it a suitable alternative to complex biosphere dynamical models. The LUE model reflects the effects of the physical and biophysical factors that determine growth rate in the concept of efficiency. The efficiency component in this model is defined as the net amount of solar energy stored by photosynthesis divided by the solar constant, and it is calculated by multiplying the geometrical, atmospheric, spectral, photochemical,

diffusion, interception, and respiration factors that reduce the efficiency component [31]. The final production of the LUE model is the net amount of solar energy stored by photosynthesis, while the essence of the final product will be changed by eliminating each factor. As it is difficult to quantify all reducing factors, a disregard for any factor causes an overestimation in the calculation of net production by the LUE model. Thus, proper model structures and rigorous model parameterization and calibration should be adopted in the modeling process. The general form of the LUE model is written as follows:

$$GPP = (fPAR) \times (PAR) \times (LUE), \quad (1)$$

in which LUE is often calculated as a function of the maximum daily light use efficiency (LUE_{max}) multiplied by environmental regulators [35]. LUE values cannot be used or compared when they are derived from different bases. Different approaches in terms of describing how LUE is controlled by ecosystem limiting factors have shaped various structures for LUE models [90]. Even having the same structure, LUE_{max} values may not match in different studies. The reason for the incompatibility of reported LUE_{max} values from different sources can be due to the data used in calibrating the model or the concepts through which fPAR was defined in each research project. In addition to different fPAR definitions, consideration of the effect of diffusive radiation on LUE_{max} has also resulted in a discrepancy in LUE_{max} reported values. In some research, an attempt was made to improve the LUE model by differentiating LUE_{max} for sunlit and shaded leaves based on the fact that diffuse radiation results in an increase of carbon uptake [91, 92].

3.1 LUE_{max} Based on Training Dataset

The LUE model has been used often for estimating GPP in the biosphere and forest ecosystems for environmental research purposes [34, 35, 93–95]. The general form of the LUE model in Eq. 1 has also been used to calculate GPP for agricultural farmlands [89]. Given that the NPP is more informative than GPP for agricultural purposes, some studies have estimated NPP using the same concept as in the LUE model as follows [96–98]:

$$NPP = (fPAR) \times (PAR) \times (LUE). \quad (2)$$

Despite that Eqs. 1 and 2 have no difference in appearance, application of the same calibrated LUE_{max} that was used for calculating GPP in this equation can cause NPP overestimation. Estimation of NPP requires the consideration of the respiration term and recalibration of the LUE parameter. It is also possible to put the dry material (DM) on the left-hand side of Eq. 1 [99], while any change in the left-hand side requires a reinterpretation of LUE_{max} .

Dry material is the dried body of a plant or a crop including stems, leaves, roots, flowers, and fruits. Neglecting the amount of NPP that is consumed by other creatures such as insects and organisms during the growth period, the DM is equal to the accumulated amount of NPP minus the weight of the liquid component of the body. Based on which parts are weighed and if the consumed portion is counted, the calibrated LUE_{max} can be case-specific. It is essential to differentiate the reported LUE_{max} values in the literature since the left-hand side of the equation may differ for different research objectives. The training dataset and the process of calibration used for the study should also be considered before applying the reported potential LUE for another study. A biome-independent LUE_{max} for NPP estimation was calibrated in the CASA model [100], while in the MODIS-GPP algorithm, LUE_{max} changes across the biome type [1, 101]. In the case of using a calibrated LUE_{max} , which has been obtained from a GPP training dataset, it is necessary to calculate and import the autotrophic respiration term in Eq. 1 and rewrite it as follows to estimate NPP:

$$NPP = (fPAR) \times (PAR) \times (LUE) - R_a. \quad (3)$$

In the MODIS daily GPP and annual NPP (MOD17A2/A3) algorithm, the annual R_a is calculated by summing the annual R_G and the annual R_M . The MOD17A2/A3 assumes that the R_G is considered to be equal with 25% of GPP and the live wood R_M is calculated using the equations that relate live wood mass to leaf mass [102].

3.2 LUE_{max} Based on the fPAR Definitions

Despite the Leaf Area Index (LAI) that ignores the complexities of canopy geometry (such as leaf angle distribution, canopy height, or shape), it is only an abstract image of the basic size of the canopy. fPAR is a radiation term that directly relates to those remotely sensed variables which are affected by the reflectance properties of different canopy structures [103]. If it is considered that the intercepted fPAR by the whole canopy contributes to the production of GPP, then fPAR is defined as $fPAR_{Canopy}$, and this concept leads LUE_{max} to be defined as $LUE_{maxCanopy}$. Through the $fPAR_{Canopy}$ concept, a sort of constant $LUE_{maxCanopy}$ values have been calculated for each of 11 biome classes and gathered into a table known as Biome-Property-Look-Up-Table (BPLUT) for the MODIS GPP/NPP algorithm [102]. The intercepted part of the incoming radiation by the non-photosynthetic part of the canopy turns to heat loss instead of GPP. Considering the photosynthetic part of the canopy as the part that can produce GPP, only the absorbed portion of $fPAR_{Canopy}$ by the chlorophyll ($fPAR_{Chl}$) is used in the LUE model and leads to a constant LUE_{maxChl} value across all biome types. $fPAR_{Chl}$ can be calculated using the Solar induced fluorescence (SIF) as a

remotely sensed proxy for the amount of chlorophyll content of the canopy as follows [35]:

$$(fPAR)_{Chl} = \frac{(SIF)}{(PAR) \times (FE)}, \quad (4)$$

where FE is the fluorescence efficiency observed at the top of the canopy.

3.3 Application of Chlorophyll Proxies in the LUE Model

Satellite chlorophyll proxies that are available for download can be categorized into two SIF and chlorophyll index products. SIF is almost equal to 1–2% of the energy absorbed by the photosynthetic part which is remitted between 734 and 758 nm by the chlorophyll content of the canopy. Interest in SIF data has grown exponentially, and the retrieval of SIF and the provision of SIF data products have become an important and formal component of spaceborne Earth observation missions [104]. Different space projects have tried to capture this fluorescence emission with various spatial and temporal resolutions (see Table 2) validated in many research studies by in situ measurements over various environments [105–108]. The SIF products are applied in the LUE model to replace $fPAR_{Canopy}$ and $LUE_{maxCanopy}$ terms with $fPAR_{Chl}$ and LUE_{maxChl} terms improving GPP estimations for global-scale environmental purposes [35]. To the best of our knowledge, the application of satellite chlorophyll proxies in the LUE model for agricultural purposes for tracing NPP, biomass, and yields in farmlands has not been assessed yet. Negligence on the application of SIF products by researchers for agricultural purposes can be due to the coarse spatial resolution of these products, especially before 2016, when 1.3 km×2.25 km (each pixel with an approximate area of 300 ha that can include variety of crops, soils and management methods in agricultural regions) was the highest available spatial resolution as show in Table 1. Possibly, it also can be due to insignificant contribution of non-photosynthetic woody limbs in crop anatomy, supposing that remote sensing of the crop canopy provides a good proxy for the crop chlorophyll content. Any probable improvement in NPP, biomass, and yield estimations on croplands using the new SIF products (with finer resolution) or the downscaled old SIF products can be investigated in future research to make decisive comments. The LUE equation for estimating GPP using the $fPAR_{Chl}$ concept is written as follows:

$$GPP = \{(fPAR)_{Chl} \times (PAR) \times (LUE)_{maxchl} \times (regulators)\} - R_a. \quad (5)$$

Regulators in Eq. 5 are the environmental factors that affect the calculation of LUE such as temperature, soil, and water [109]. As NPP has always been the case for agricultural studies, Eq. 5 can be written as:

Table 2 Satellite products of NASA and European space agency for chlorophyll proxies and their spatiotemporal resolution. Continuity to the MTCI is provided by OLCI on-board the Sentinel-3 missions from 2016 with a much higher spatiotemporal resolution

Chlorophyll proxies	Resolution		Available date	Data openly available	
	Spatial	Temporal			
Greenhouse Gases Observing Satellite (GOSAT)	82 km ² per sounding (~ 10 km diameter)	3 days	Since 2009	https://data.caltech.edu/records/rt4es-7m264	
SIF product	GOME-2 SIF	0.5° × 0.5°	Daily	Since 2007	https://avdc.gsfc.nasa.gov/pub/data/satellite/MetOp/GOME_F/
	COC-2 SIF	1.3 km × 2.25 km	16 days	Since 2014	https://disc.gsfc.nasa.gov/datasets/OCO2_L2_Lite_SIF_10r/summary?keywords=oco2%20sif%20lite
	OCO-3 SIF	1.3 km × 2.25 km	16 days	Since 2019	https://disc.gsfc.nasa.gov/datasets/OCO3_L2_Lite_SIF_10r/summary
	OLCI SIF	300 m × 300 m	2 days	Since 2016	https://apps.sentinel-hub.com/eo-browser
	TROPISIF (Sentinel-5P TROPOMI mission)	7.5 km × 3.5 km	Daily	Since 2018	https://s5p-tropisif.noveltis.fr/data-access/
Chlorophyll index	MTCI	0.5° × 0.5°	Decay	2002–2012	https://data.ceda.ac.uk/neodc/mtci/data
	OTCI	300 m × 300 m	2 days	Since 2016	https://apps.sentinel-hub.com/eo-browser/

$$NPP = (fPAR)_{Chl} \times (PAR) \times (LUE)_{maxChl} \times (\text{regulators}). \quad (6)$$

In Eq. 6, the LUE_{maxChl} parameter can be calibrated using NPP training dataset. It should be investigated if Eq. 6 ($fPAR_{Chl}$ and LUE_{maxChl} concepts) could contribute to improve NPP estimation on farmlands in agricultural research. Given that traditional vegetation indices (VIs) tend to exhibit saturation effects in dense canopies and considering the high correlation between satellite SIF datasets and crop productivity [110], it is recommended to test the use of SIF products in estimating crop production to explore their potential for improving accuracy in such estimations. The test may require the use of a downscaled version of the SIF products as the spatial resolution of the available SIF products (especially before 2016) does not allow researchers to calibrate LUE_{maxChl} for specific crops (one pixel may cover different types of land use).

3.4 Downscaled Version of the SIF Products

3.4.1 Regression Approach

Apparent canopy SIF yield of corn, soybean, forest, and grass/pasture from two satellite instruments, OCO-2 and TROPOMI, showed clear seasonal and spatial patterns [111]. This suggests that the ability of SIF to observe spatial variances is worth considering despite the coarse resolution of some SIF products. Despite the development of new SIF products with fine resolutions, the endeavor to use coarse products is still ongoing

due to a lack of continuous satellite SIF data for long-term evaluations [112]. One of the approaches to deal with the spatial coarseness of the remote sensing products is downscaling [113]. In the context of remote sensing, downscaling refers to a decrease in the pixel size of remotely sensed images; this is a scaling process, converting from a low to a high spatial resolution preserving the original image radiometry. Simplistically, the average of the simulated high-resolution subpixel values is equal to the pixel value of the original low-resolution image. The effective emissivity is derived from the high-resolution NDVI-composite image which has been used as the scaling factor to downscale the LST image [114]. Along with the same concept, the following equation downscales a SIF pixel with 0.05° spatial resolution (from GOME-2) using the number of NDVI pixels with 250 m spatial resolution (obtained from bands 1 and 2 of MODIS) covered by the SIF pixel:

$$(SIF)_{250m} = (SIF)_{0.05^\circ} \times \frac{(NDVI)_{250m}}{(NDVI)_{0.05^\circ}}, \quad (7)$$

where SIF_{250m} is the downscaled SIF pixel with 250 m spatial resolution, $SIF_{0.05^\circ}$ is the original SIF pixel with 0.05° spatial resolution, $NDVI_{250m}$ is the NDVI pixel calculated by red and near infrared bands of the MODIS with 250 m spatial resolution, and $NDVI_{0.05^\circ}$ is the NDVI pixel with 0.05° spatial resolution obtained from averaging $NDVI_{250m}$ pixels underlaid the original SIF pixel. Both $SIF_{0.05^\circ}$ and $NDVI_{250m}$ pixels should correspond to similar weather conditions, so the downscaling process requires images of the same dates. In another method, a linear regression model is established in

the downscaling procedure [115]. After plotting $SIF_{0.05^\circ}$ pixels against $NDVI_{0.05^\circ}$ pixels, the following equation is fitted:

$$(SIF)_{0.05^\circ} = a + b \times (NDVI)_{0.05^\circ}. \quad (8)$$

Assuming that inside a $SIF_{0.05^\circ}$ pixel the regression equation for SIF_{250m} pixels versus $NDVI_{250m}$ pixels has the same coefficients with Eq. 8, then it can be written as:

$$(SIF)_{250m} = a + b \times (NDVI)_{250m}. \quad (9)$$

The following revision is required on SIF_{250m} pixels to preserve Eq. 8 for the downscaled SIF image:

$$(SIF)_{250m}^r = (SIF)_{250m} \pm \sigma, \quad (10)$$

where SIF_{250m}^r is the revised value of SIF_{250m} and σ is calculated using the following equation:

$$\sigma = (SIF)_{0.05^\circ} - (SIF)_{0.05^\circ}^{avg}, \quad (11)$$

where $SIF_{0.05^\circ}^{avg}$ is the average of the SIF_{250m} in pixels underlaid a $SIF_{0.05^\circ}$ pixel:

$$(SIF)_{0.05^\circ}^{avg} = \frac{\sum_1^q (SIF)_{250m}}{q}, \quad (12)$$

where q is the number of pixels underlaid a $SIF_{0.05^\circ}$ pixel.

3.4.2 Area-to-Point Regression Kriging

Downscaling changes the size associated with each data value (support) which means that in geostatistics, it can be considered as a change of support problem (COSP). The GSOP is concerned with inference about the values of a variable at points (point-referenced or simply point data) or blocks (block data) different from those at which it was observed [116]. Kriging processes have been applied to take the kriged values for the blocks (larger support) from the point-level observations (point-to-area prediction) [117] and reversely to predict a support that is smaller than that of the original data (area-to-point prediction) applicable for the downscaling procedure [118]. For example, one might be interested in the significance of the correlation between point observations (point support) and data derived from a regional model (areal support). In such cases, the latter areal support predictions must also be transformed to the point support level coherently in a way that these point support predictions can reproduce exactly the corresponding areal data when they are convolved with the discrete sampling kernel (convolution kernel). The uncertainty in downscaled data derived from coarser resolution using area-to-point approach can be assessed in a Monte Carlo framework [119]. In remote sensing, since values lie in similar supports (pixels of the same size), the

problem is simpler than for the cases with irregular supports (like zips in a census or hydrologic response units in a semi distributed model) [120].

The prediction of area-to-point regression kriging (ATPRK) for fine pixels $Z_v^l(x)$ of band k underlaid the coarse pixels $Z_v^l(x)$ of band l is [113]:

$$Z_v^l(x) = Z_v^l(x) + Z_{v2}^l(x) \quad (13)$$

where $Z_{v1}^l(x)$ and $Z_{v2}^l(x)$ are the predictions of the regression and ATPRK parts. The regression part takes advantage of fine ancillary data. For example, in case of downscaling a coarse band of MODIS, one of the fine bands with the greater correlation coefficient can be selected as a band that provides ancillary data to be fused for the coarse band. $Z_{v1}^l(x)$ is the prediction of the linear regression between the coarse band Z_v^l and its corresponding ancillary fine band Z_v^{lk} (used as covariate) that can be calculated as follows;

$$Z_{v1}^l(x) = a_1 \times Z_v^{lk}(x) + b_1. \quad (14)$$

To estimate a_1 and b_1 , Eq.15 assumed to be exist at coarse spatial resolution:

$$Z_{v1}^l(x) = a_1 \times Z_v^{lk}(x) + b_1, \quad (15)$$

where $Z_v^{lk}(x)$ is the coarse image produced by upscaling Z_v^{lk} using the point spread function (PSF) and the convolution operator. The residuals of the regression should be calculated to reproduce the spectral properties of the observed coarse data. ATPRK part downscales the residuals $Z_{v2}^l(x)$ to fine spatial resolution residuals $Z_{v2}^l(x)$. Based on ATPRK, the fine residual $Z_{v2}^l(x)$ is a linear combination of N coarse residuals of band l :

$$Z_{v2}^l(x) = \sum_{i=1}^N (\lambda_i \times Z_{v2}^l(x_i)), \text{ s.t. } \sum_{i=1}^N \lambda_i = 1, \quad (16)$$

where λ_i is the weight vector $\{\lambda_1, \dots, \lambda_N\}$ that yields the minimum prediction error variance among all weighed linear combinations of N coarse residuals. λ_i is obtained from the corresponding kriging system consists of coarse-to-coarse residual covariance between coarse pixels, fine-to-coarse residual covariance between fine and coarse pixels, and the Lagrange multipliers. The N coarse residuals are from the N coarse pixels surrounding the pixel in a $N \times N$ window. In case the area-to-point regression kriging method is used to downscale a coarse SIF image, a finer $NDVI$ image obtained from MODIS or Landsat bands can provide the required ancillary data.

3.4.3 Super-Resolution Mapping

Super-resolution mapping (SRM) uses auxiliary data to increase the spatial resolution of each pixel based on the

classification techniques [121]. The objective is to increase the spatial resolution of an image with a coarse spatial resolution using other image(s) with the desired fine spatial resolution but of a different spectral band(s) [122]. Unlike hard classification approaches that assign one class for each pixel, soft classification approaches predict the proportional cover of each land cover class within each pixel. However, the location of the land cover classes in the mixed pixels (the spatial resolution of the thematic map) is not increased relative to that of hard classification. SRM predicts the location of land cover classes within a pixel based on the proportion images produced by soft classification using different approaches like image fusion [123]. Since soft classification methods are limited in terms of detail and accuracy of the resulting thematic map, it is suggested the information available at a finer spatial resolution should be used. Several sources of information at a finer resolution are geostatistical data, fused images, and panchromatic imagery [124]. A proliferation of SRM methods includes artificial neural networks, subpixel-swapping methods, spatial attraction models, Markov random fields, geostatistical solutions, interpolation-based approaches, and other advanced methods [125].

Generally, an SRM analysis has two main steps: first downscaling the coarse resolution fraction image to a fine spatial resolution indicator image which represents the possibility of each fine resolution pixel belonging to a specified land cover class and, second, combining fine fraction images to produce a fine resolution land cover map [126]. SRM models use different techniques for the downscaling step. SRM models based on spatial dependence that define the spatial pattern explicitly may be inadequate for the representation of complex land cover mosaics for which a learning-based model may work better in SRM [127, 128]. The aim of a learning-based model like back-propagation

neural networks and support vector regression is to learn the spatial pattern of land cover from existing fine-resolution land cover maps assuming that the pattern is constant while their performance is limited in the case of existing complex nonlinear relationships between the coarse and fine resolution data [126]. Deep learning methods have been shown to have considerable potential in SRM to produce more accurate maps than traditional machine learning approaches [129]. Figure 3 shows a schematic of a SRM process through which a downscaled pixel is produced from the proportion image and the auxiliary pixels. In the case of downscaling a coarse SIF image, the SIF image is used to produce proportion images, and the next one or multiple auxiliary images such as a panchromatic image or a vegetation index image obtained from other satellites with higher resolution can be tested in RSM. By evaluating the downscaled SIF images obtained from the application of different sets of auxiliary images, the best set of auxiliary images for downscaling SIF images can be determined.

3.4.4 Long-Term Temporally Corrected and Spatially Downscaled SIF Product

Due to the temporal inconsistency induced by sensor degradation and to correct the impacts of the degradation, generation of long-term temporally corrected and spatially downscaled SIF products is one of the latest attempts in making the SIF products practical for studies [112]. The process includes three main steps: spatial downscaling, temporal correction, and multi-sensor fusion. The process led to generate a long-term temporally corrected SIF product from July 1995 to December 2018 with a high spatial resolution (0.05°). Downscaling phase can be conducted using the LUE-based method and machine learning methods [130, 131].

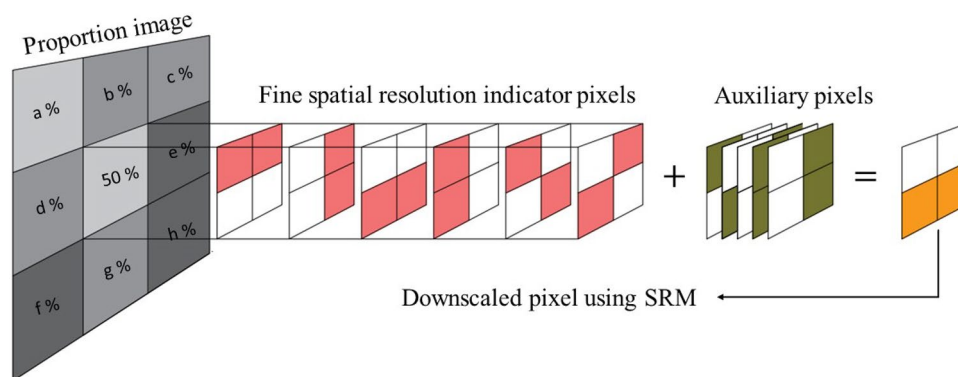


Fig. 3 A schematic of a downscaled pixel using RSM, assuming that the goal is to increase the resolution of a coarse pixel by 4 times according to the resolution of the existing auxiliary pixels. It is also assumed that the proportional value of the coarse pixel is estimated to 50% in the proportional image. Based on the above assumptions, 6

modes can be imagined for the downscaled pixel, and the downscaled pixel is one of these modes. An auxiliary pixel or auxiliary pixels are used to determine one of the modes with the highest probability as the downscaled pixel

To conduct temporal correction phase, a long-term time series of satellite SIF in a region as the benchmark is required to correct the trend. A stable desert with a very sparse vegetation is recommended as a benchmark since the SIF signals is expected to be very small and constant across the recent years in such a land cover [112]. Average monthly time series of satellite SIF are extracted for the benchmark to get the normalized SIF time series which is used for correcting the temporal trend of satellite SIF. Finally, cumulative distribution frequency (CDF) matching approach is used to fuse these three independent SIF datasets into a long-term consistent data record [131].

4 Functional Models

Functional models are simplified versions of the complex mechanistic models or a combination with statistical schemes and are more suitable for operational crop yield forecasting due to their minimal data input requirements, and the key processes can be parametrized using approximate equations [48, 132]. In recent years, functional models have tended to integrate both climate and remote sensing indices into unified yield prediction models [133–136]. Functional models can be trained through a single predictor regression, a multiple linear regression, or a nonlinear relation analysis approach [54, 55, 60,). Along with the agricultural perspective, functional models in combination with forecast statistical algorithms are used for yield forecasting and produce early warnings [48]. Figure 4 is a flow inferred from the reviewed research to show the contribution of statistical and mechanistic models and remote sensing data in a functional model that can estimate NPP and yield values and produce early warning for yield reduction before harvest.

4.1 Different Methods in Functional Models

Functional models include different approaches through which process-based methods are combined with remotely sensed data. Figure 5 describes one of these approaches based on an empirical equation between fPAR and LAI [55]. According to the proposed methodology, LUE is calibrated using the data obtained from running a crop model. The model is run for different scenarios for each DOY to estimate NPP and LAI values for that DOY. The NPP and LAI values for each DOY obtained from the crop model are shown with CM subscript (NPP_{CM} and LAI_{CM} , respectively). Several values for NPP_{CM} and LAI_{CM} are calculated based on different scenarios on each DOY for which the $(R^2)_{Year1,DOY1}$ value is obtained by plotting them versus each other. The process is applied for different years for which the required key parameters for running the crop model are available. The highest amount of R^2 determines the DOY on which the LAI (shown with LAI_{Best}) returns the best estimation of NPP. The LAI_{Best} value returns the fPAR value using a linear equation which is shown with CM subscript ($fPAR_{CM}$) since it is obtained from running a crop model. Using the $fPAR_{CM}$ value, LUE_{CM} is calculated by the LUE equation. Finally, the NPP value for each pixel (NPP_{CM+RS}) is calculated from the calibrated LUE value (LUE_{CM}) and the remotely sensed fPAR value ($fPAR_{RS}$) using the LUE equation.

Figure 6 shows another approach for building a functional model based on converting LAI_{CM} to pseudo-LAI observations (LAI_{PO}) and a multiple linear regression equation [54]. The proposed method provides a way to estimate the spatiotemporal distribution of the NPP values using remotely sensed vegetation indexes integrated with weather data. In the first step, the LAI values obtained from a crop model are converted to pseudo-vegetation

Fig. 4 Development of the concept of functional model through the incorporation of statistical and mechanistic models, as well as the utilization of remote sensing data to estimate spatiotemporal distribution of NPP and yield values and its combination with forecasting algorithms to produce early warnings for probable yield reduction before harvest (inferred from the reviewed research)

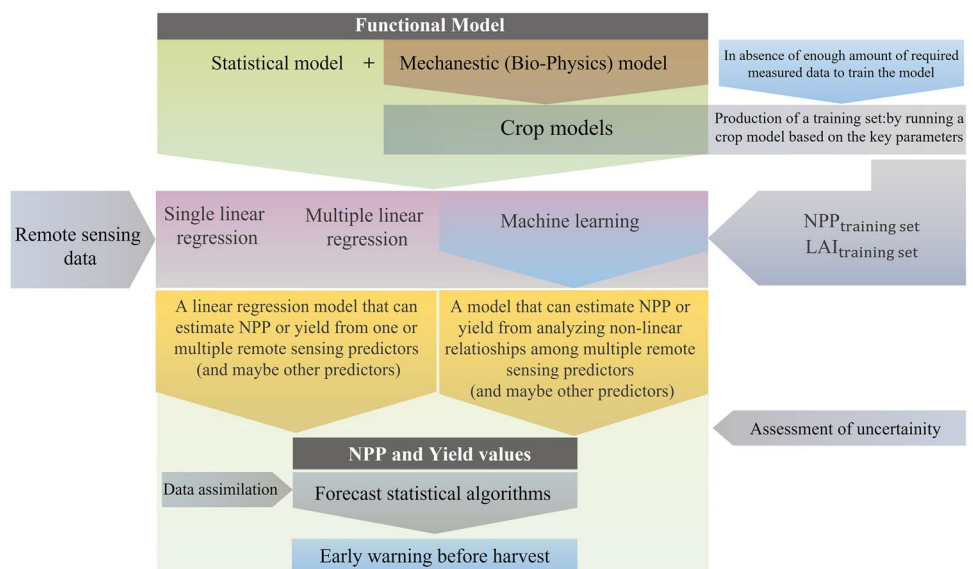
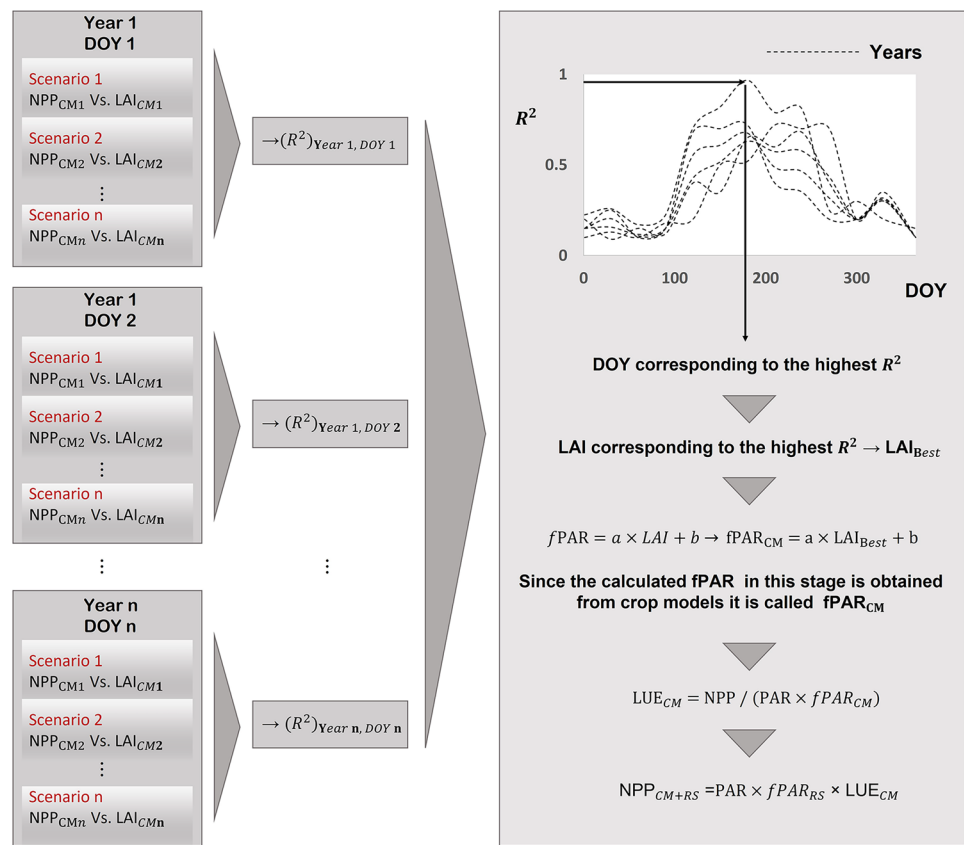


Fig. 5 A proposed process for estimating the spatiotemporal distribution of NPP values in which LUE is calibrated by the data obtained from running a crop model for several scenarios. The calibrated LUE is used in integration with the fPAR product of satellites to calculate NPP for each pixel



index observations using empirical equations. The pseudo-values are used to calibrate the coefficients of a multiple linear regression model after which the real remotely sensed values of a vegetation index are imported into the model to calculate the NPP_{CM+RS} values. Instead of training a simple linear or multiple linear regression equation, grid data on crop yield, remotely sensed data, and climate data can be used to train a machine learning method such as the deep learning algorithm to estimate crop yield [137].

4.2 Application of Chlorophyll Proxies in Functional Models

Based on the promising results obtained from the use of chlorophyll proxies in estimating GPP using LUE models, the present paper proposes the evaluation of these proxies in functional models in estimating NPP and yield for agricultural purposes. Application of chlorophyll proxies in functional models can be followed by introducing new NPP and yield chlorophyll-based predictors for these models. The proposed predictors that can be evaluated in future studies in estimating NPP and yield can be a chlorophyll index or a multiplied sentence including $fPAR_{Chl}$. The proposed predictors can be used to build a single linear regression model shown in Eqs. 17 and 18.

$$NPP = a \times (Chl) + b, \tag{17}$$

$$NPP = a \times (fPAR)_{Chl} \times (PAR) \times (LUE)_{maxChl} + b, \tag{18}$$

where Chl is the chlorophyll index such as MTCI and OTCI, $fPAR_{Chl}$ is the fPAR relating to chlorophyll content of the canopy and LUE_{maxChl} is the maximum daily LUE based on PAR absorption by canopy chlorophyll. The predictors can be used in a multiple linear regression model shown in Eqs. 19 and 20. In a multiple linear regression model, a chlorophyll-based predictor can be integrated with other predictors (P) as below:

$$NPP = a_1 \times (Chl) + a_2 \times P + a_3, \tag{19}$$

$$NPP = a_1 \times (fPAR)_{Chl} \times (PAR) \times (LUE)_{maxChl} + a_2 \times P + a_3. \tag{20}$$

Since the amount of actual evapotranspiration in the anthesis stage ($ET_{Anthesis}$) has been recognized as a differentiating factor to categorize wheat fields into high-productive and low-productive classes [138], a model in which P is replaced by $ET_{Anthesis}$ can be evaluated for estimating yield before harvest. Remotely sensed chlorophyll-based predictors in addition to other predictors relating to weather, soil type, soil moisture,

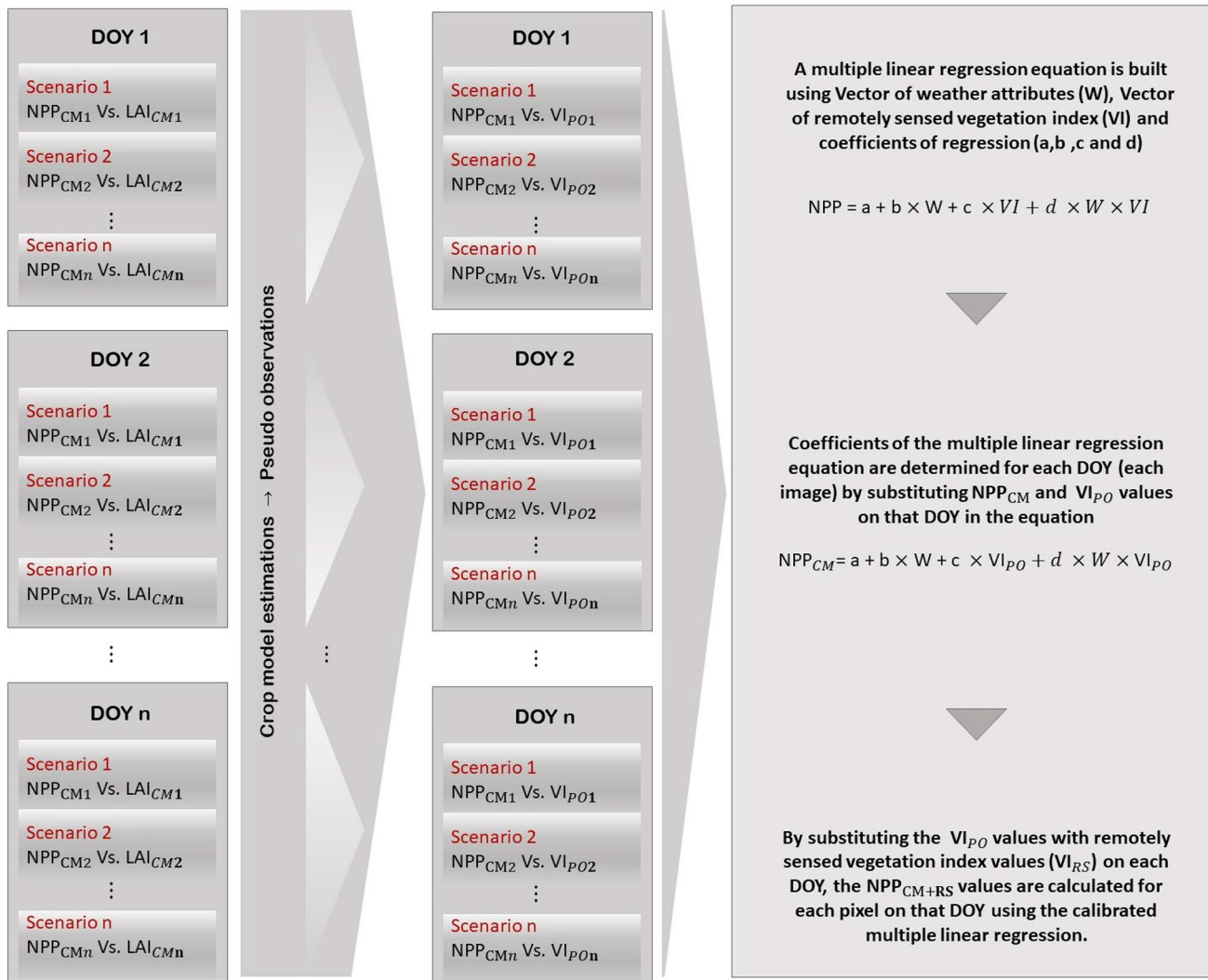


Fig. 6 A proposed process for estimating the spatiotemporal distribution of NPP values in which a multiple linear regression equation is calibrated using pseudo-vegetation index observations

topography, fertilizers, pesticides, etc. can also be used to train a complex machine learning model for further investigation of NPP and yield estimation. Despite an observed strong seasonal correlation between SIF and GPP, changes in plant growth stages can affect this relationship. Recently, the relationship is investigated for maize from C4 plant category, and it has found that canopy structure impacts seasonal variations of SIF and its relation to GPP [36]. It has been found that exponential regression is the best method to capture the nonlinearity at the site level, while the degree of the nonlinearity varies among different biomes [139]. Indeed, SIF-GPP relationships tend to vary not only between vegetation types but also between crop species specifically [140]. However, additional measurements for different vegetation types are necessary for fully understanding the effects of factors on SIF signals for on croplands. The fact that the relationship between SIF and photosynthesis

changes both seasonally and by events may lead to test the nonlinear functions or non-constant coefficients in building functional models for future studies.

5 Conclusion

A comprehensive overview and categorization of the literature that include GPP and NPP studies were presented to clarify the different approaches applied to estimate GPP and its derivatives with environmental and agricultural purposes. From an environmental perspective, GPP as the output from dynamic global vegetation models was reviewed to identify its role in quantification of vegetation production and in simulation of ecosystem processes and the hydro-biochemical cycle [141]. The terrestrial carbon cycle

also can be traced using the simple LUE model instead of multiparameter complex models [89]. Application of the LUE model for quantification of GPP in the biosphere has improved by introducing $fPAR_{Chl}$ and LUE_{Chl} concepts based on remotely sensed SIF products [35]. The review indicated that just as the GPP estimations are important for environmental purposes, so are its derivatives, NPP, biomass, and yield for agricultural purposes where attempts have focused on crop yield predictions made before harvest [48, 138]. The review showed that the LUE model, crop models, statistical models, and their incorporation into so-called functional models are the common approaches for estimating the NPP as the most important derivative of GPP in agricultural perspective. Due to a promising application of chlorophyll proxies in the utilization of the LUE model at global scale environmental studies for estimating GPP [35], this study proposes the test of these proxies in regional scale agricultural studies for estimating NPP, biomass, and yield. In the process of estimating NPP using chlorophyll proxies, coarseness of the spatial resolution of historical remotely sensed SIF products can limit their application for agricultural purposes. Hence, different downscaling methodologies that can be used in the downscaling process of the SIF products were reviewed. Generation of long-term temporally corrected and spatially downscaled SIF product with cumulative distribution frequency (CDF) matching approach was of the latest attempts to increase the resolution of SIF products up to 0.05° [112, 131].

With the increase in access to high resolution products of SIF and chlorophyll proxies, the present review paper proposed their application for being tested in both the LUE and functional models for estimating NPP, biomass and yield in agricultural studies. Since different functional models can be built by different combinations of predictors including ground measured or remote sensing predictors, introducing any new remote sensing predictor that can reduce dependency on the field measured data is useful to fulfill the objective of the functional model. Non-linearity generally exists between total emitted SIF and GPP at the canopy level that may require the change of the proposed linear equations into nonlinear forms or employment of different coefficients for crop growth stages. Hence, future studies on testing remote sensing chlorophyll-based predictors will make it clear if they are able to increase the accuracy of NPP estimations with the LUE model or reduce the dependency of functional models on field measured data.

Author Contribution Hamed Sabzchi-Dehkharghania wrote the main text. Asim Biswas, Sarita Gajbhiye Meshram, and Abolfazl Majnooni-Heris contributed to the review of the paper.

Availability of Data and Materials Data sharing is not applicable to this article as no new data were created or analyzed in this study.

Declarations

Ethics Approval No approval of research ethics committees was required.

Competing Interests The authors declare no competing interests.

References

- Running, S.W., Thornton, P.E., Nemani, R. & Glassy, J.M. (2000). Global terrestrial gross and net primary productivity from the earth observing system. *In Methods in ecosystem science*, 44–57. Springer, New York, NY. https://doi.org/10.1007/978-1-4612-1224-9_4
- Dimitrov, D.D., Grant, R.F., Lafleur, P.M. & Humphreys, E.R. (2011). Modeling the effects of hydrology on gross primary productivity and net ecosystem productivity at Mer Bleue Bog. *Journal of Geophysical Research: Biogeosciences*, 116(G4). <https://doi.org/10.1029/2010JG001586>
- Fatichi, S., Zeeman, M. J., Fuhrer, J., & Burlando, P. (2014). Ecohydrological effects of management on subalpine grasslands: From local to catchment scale. *Water Resources Research*, 50(1), 148–164. <https://doi.org/10.1002/2013WR014535>
- Gan, R., Zhang, Y., Shi, H., Yang, Y., Eamus, D., Cheng, L., Chiew, F.H. & Yu, Q. (2018). Use of satellite leaf area index estimating evapotranspiration and gross assimilation for Australian ecosystems. *Ecohydrology*, 11(5), p.e1974. <https://doi.org/10.1002/eco.1974>
- Govind, A., Chen, J. M., McDonnell, J., Kumari, J., & Sonnentag, O. (2011). Effects of lateral hydrological processes on photosynthesis and evapotranspiration in a boreal ecosystem. *Ecohydrology*, 4(3), 394–410. <https://doi.org/10.1002/eco.141>
- Manoli, G., Mejjide, A., Huth, N., Knohl, A., Kosugi, Y., Burlando, P., Ghazoul, J. & Fatichi, S. (2018). Ecohydrological changes after tropical forest conversion to oil palm. *Environmental Research Letters*, 13(6), p.064035. <https://doi.org/10.1088/1748-9326/aac54e>
- van Schaik, E., Killaars, L., Smith, N. E., Koren, G., Van Beek, L. P. H., Peters, W., & van der Laan-Luijkx, I. T. (2018). Changes in surface hydrology, soil moisture and gross primary production in the Amazon during the 2015/2016 El Niño. *Philosophical Transactions of the Royal Society B: Biological Sciences*, 373(1760), 20180084. <https://doi.org/10.1098/rstb.2018.0084>
- Law, B. E., Ryan, M. G., & Anthoni, P. M. (1999). Seasonal and annual respiration of a ponderosa pine ecosystem. *Global Change Biology*, 5(2), 169–182. <https://doi.org/10.1046/j.1365-2486.1999.00214.x>
- da Costa, A. C., Metcalfe, D. B., Doughty, C. E., de Oliveira, A. A., Neto, G. F., da Costa, M. C., Silva Junior, J. D. A., Aragão, L. E., Almeida, S., Galbraith, D. R., & Rowland, L. M. (2014). Ecosystem respiration and net primary productivity after 8–10 years of experimental through-fall reduction in an eastern Amazon forest. *Plant Ecology & Diversity*, 7(1–2), 7–24. <https://doi.org/10.1080/17550874.2013.798366>
- Goulden, M. L., McMillan, A. M. S., Winston, G. C., Rocha, A. V., Manies, K. L., Harden, J. W., & Bond-Lamberty, B. P. (2011). Patterns of NPP, GPP, respiration, and NEP during boreal forest succession. *Global Change Biology*, 17(2), 855–871. <https://doi.org/10.1111/j.1365-2486.2010.02274.x>
- Kirschbaum, M.U.F., Eamus, D., Gifford, R.M., Roxburgh, S.H. & Sands, P.J. (2001). Definitions of some ecological terms commonly used in carbon accounting. *Cooperative Research Centre for Carbon Accounting, Canberra*, 2–5.
- Chapin, F. S., III., & Eviner, V. T. (2003). Biogeochemistry of terrestrial net primary production. *Treatise on geochemistry*, 8, 682.
- Neumann, M., Zhao, M., Kindermann, G., & Hasenauer, H. (2015). Comparing MODIS net primary production estimates

- with terrestrial national forest inventory data in Austria. *Remote Sensing*, 7(4), 3878–3906.
14. Niedertscheider, M., Kastner, T., Fetzl, T., Haberl, H., Kroisleitner, C., Plutzer, C. & Erb, K.H. (2016). Mapping and analysing cropland use intensity from a NPP perspective. *Environmental Research Letters*, 11(1), 014008. <https://doi.org/10.1088/1748-9326/11/1/014008>
 15. Peng, D., Huang, J., Li, C., Liu, L., Huang, W., Wang, F., & Yang, X. (2014). Modelling paddy rice yield using MODIS data. *Agricultural and Forest Meteorology*, 184, 107–116. <https://doi.org/10.1016/j.agrformet.2013.09.006>
 16. Waring, R. H., Landsberg, J. J., & Williams, M. (1998). Net primary production of forests: A constant fraction of gross primary production? *Tree physiology*, 18(2), 129–134. <https://doi.org/10.1093/treephys/18.2.129>
 17. Gifford, R.M. (1995). Whole plant respiration and photosynthesis of wheat under increased CO₂ concentration and temperature: Long-term vs. short-term distinctions for modelling. *Global Change Biology*, 1(6), 385–396. <https://doi.org/10.1111/j.1365-2486.1995.tb00037.x>
 18. Bond-Lamberty, B., Bailey, V. L., Chen, M., Gough, C. M., & Vargas, R. (2018). Globally rising soil heterotrophic respiration over recent decades. *Nature*, 560(7716), 80–83. <https://doi.org/10.1038/s41586-018-0358-x>
 19. Krinner, G., Viovy, N., de Noblet-Ducoudré, N., Ogée, J., Polcher, J., Friedlingstein, P., Ciais, P., Sitch, S. & Prentice, I.C. (2005). A dynamic global vegetation model for studies of the coupled atmosphere-biosphere system. *Global Biogeochemical Cycles*, 19(1). <https://doi.org/10.1029/2003GB002199>
 20. Peng, C. (2000). From static biogeographical model to dynamic global vegetation model: A global perspective on modelling vegetation dynamics. *Ecological modelling*, 135(1), 33–54. [https://doi.org/10.1016/S0304-3800\(00\)00348-3](https://doi.org/10.1016/S0304-3800(00)00348-3)
 21. Zhuang, Q., He, J., Lu, Y., Ji, L., Xiao, J., & Luo, T. (2010). Carbon dynamics of terrestrial ecosystems on the Tibetan Plateau during the 20th century: An analysis with a process-based biogeochemical model. *Global Ecology and Biogeography*, 19(5), 649–662. <https://doi.org/10.1111/j.1466-8238.2010.00559.x>
 22. Running, S. W., Baldocchi, D. D., Turner, D. P., Gower, S. T., Bakwin, P. S., & Hibbard, K. A. (1999). A global terrestrial monitoring network integrating tower fluxes, flask sampling, ecosystem modeling and EOS satellite data. *Remote sensing of environment*, 70(1), 108–127. [https://doi.org/10.1016/S0034-4257\(99\)00061-9](https://doi.org/10.1016/S0034-4257(99)00061-9)
 23. Keenan, T. F., Migliavacca, M., Papale, D., Baldocchi, D., Reichstein, M., Torn, M., & Wutzler, T. (2019). Widespread inhibition of daytime ecosystem respiration. *Nature ecology & evolution*, 3(3), 407–415. <https://doi.org/10.1038/s41559-019-0809-2>
 24. Zhan, W., Yang, X., Ryu, Y., Dechant, B., Huang, Y., Goulas, Y., Kang, M. & Gentine, P. (2022). Two for one: Partitioning CO₂ fluxes and understanding the relationship between solar-induced chlorophyll fluorescence and gross primary productivity using machine learning. *Agricultural and Forest Meteorology*, 321, 108980. <https://doi.org/10.1016/j.agrformet.2022.108980>
 25. Raoult, N., Delorme, B., Otlé, C., Peylin, P., Bastrikov, V., Maugis, P., & Polcher, J. (2018). Confronting soil moisture dynamics from the ORCHIDEE land surface model with the ESA-CCI Product: Perspectives for data assimilation. *Remote Sensing*, 10(11), 1786. <https://doi.org/10.3390/rs10111786>
 26. Sitch, S., Huntingford, C., Gedney, N., Levy, P. E., Lomas, M., Piao, S. L., Betts, R., Ciais, P., Cox, P., Friedlingstein, P., & Jones, C. D. (2008). Evaluation of the terrestrial carbon cycle, future plant geography and climate-carbon cycle feedbacks using five Dynamic Global Vegetation Models (DGVMs). *Global change biology*, 14(9), 2015–2039. <https://doi.org/10.1111/j.1365-2486.2008.01626.x>
 27. Ngo-Duc, T., Laval, K., Ramillien, G., Polcher, J. & Cazenave, A. (2007). Validation of the land water storage simulated by Organising Carbon and Hydrology in Dynamic Ecosystems (ORCHIDEE) with Gravity Recovery and Climate Experiment (GRACE) data. *Water Resources Research*, 43(4). <https://doi.org/10.1029/2006WR004941>
 28. Arora, V. (2002). Modeling vegetation as a dynamic component in soil-vegetation-atmosphere transfer schemes and hydrological models. *Reviews of Geophysics*, 40(2), 3–1. <https://doi.org/10.1029/2001RG000103>
 29. Franks, S. W., Beven, K. J., Quinn, P. F., & Wright, I. R. (1997). On the sensitivity of soil-vegetation-atmosphere transfer (SVAT) schemes: Equifinality and the problem of robust calibration. *Agricultural and Forest Meteorology*, 86(1–2), 63–75. [https://doi.org/10.1016/S0168-1923\(96\)02421-5](https://doi.org/10.1016/S0168-1923(96)02421-5)
 30. Gerten, D., Schaphoff, S., Haberlandt, U., Lucht, W., & Sitch, S. (2004). Terrestrial vegetation and water balance—hydrological evaluation of a dynamic global vegetation model. *Journal of hydrology*, 286(1–4), 249–270. <https://doi.org/10.1016/j.jhydrol.2003.09.029>
 31. Monteith, J. L. (1972). Solar radiation and productivity in tropical ecosystems. *Journal of applied ecology*, 9(3), 747–766.
 32. Liu, L., & Cheng, Z. (2010). Detection of vegetation light-use efficiency based on solar-induced chlorophyll fluorescence separated from canopy radiance spectrum. *IEEE Journal of Selected Topics in Applied Earth Observations and Remote Sensing*, 3(3), 306–312. <https://doi.org/10.1109/JSTARS.2010.2048200>
 33. Xiao, X. (2006). Light absorption by leaf chlorophyll and maximum light use efficiency. *IEEE Transactions on Geoscience and Remote Sensing*, 44(7), 1933–1935. <https://doi.org/10.1109/TGRS.2006.874796>
 34. Zhang, Q., Middleton, E. M., Margolis, H. A., Drolet, G. G., Barr, A. A., & Black, T. A. (2009). Can a satellite-derived estimate of the fraction of PAR absorbed by chlorophyll (FAPARchl) improve predictions of light-use efficiency and ecosystem photosynthesis for a boreal aspen forest? *Remote Sensing of Environment*, 113(4), 880–888. <https://doi.org/10.1016/j.rse.2009.01.002>
 35. Zhang, Y., Xiao, X., Wolf, S., Wu, J., Wu, X., Gioli, B., Wohlfahrt, G., Cescatti, A., Van der Tol, C., Zhou, S., & Gough, C. M. (2018). Spatio-temporal convergence of maximum daily light-use efficiency based on radiation absorption by canopy chlorophyll. *Geophysical research letters*, 45(8), 3508–3519. <https://doi.org/10.1029/2017GL076354>
 36. Li, Z., Zhang, Q., Li, J., Yang, X., Wu, Y., Zhang, Z., Wang, S., Wang, H. & Zhang, Y. (2020). Solar-induced chlorophyll fluorescence and its link to canopy photosynthesis in maize from continuous ground measurements. *Remote Sensing of Environment*, 236, 111420. <https://doi.org/10.1016/j.rse.2019.111420>
 37. de Vries, W., Posch, M., Simpson, D., & Reinds, G. J. (2017). Modelling long-term impacts of changes in climate, nitrogen deposition and ozone exposure on carbon sequestration of European forest ecosystems. *Science of the Total Environment*, 605, 1097–1116. <https://doi.org/10.1016/j.scitotenv.2017.06.132>
 38. Fernández-Martínez, M., Vicca, S., Janssens, I. A., Campioli, M., & Penuelas, J. (2016). Nutrient availability and climate as the main determinants of the ratio of biomass to NPP in woody and non-woody forest compartments. *Trees*, 30(3), 775–783. <https://doi.org/10.1007/s00468-015-1319-8>
 39. Liebhold, A. M., Brockerhoff, E. G., Kalisz, S., Nuñez, M. A., Wardle, D. A., & Wingfield, M. J. (2017). Biological invasions in forest ecosystems. *Biological Invasions*, 19(11), 3437–3458. <https://doi.org/10.1007/s10530-017-1458-5>
 40. Petrie, M. D., Collins, S. L., Swann, A. M., Ford, P. L., & Litvak, M. E. (2015). Grassland to shrubland state transitions enhance carbon sequestration in the northern Chihuahuan Desert. *Global Change Biology*, 21(3), 1226–1235. <https://doi.org/10.1111/gcb.12743>

41. De Leeuw, J., Rizayeva, A., Namazov, E., Bayramov, E., Marshall, M. T., Etzold, J., & Neudert, R. (2019). Application of the MODIS MOD 17 Net Primary Production product in grassland carrying capacity assessment. *International Journal of Applied Earth Observation and Geoinformation*, 78, 66–76. <https://doi.org/10.1016/j.jag.2018.09.014>
42. Maselli, F., Argenti, G., Chiesi, M., Angeli, L., & Papale, D. (2013). Simulation of grassland productivity by the combination of ground and satellite data. *Agriculture, ecosystems & environment*, 165, 163–172. <https://doi.org/10.1016/j.agee.2012.11.006>
43. Tian, H., Chen, G., Liu, M., Zhang, C., Sun, G., Lu, C., Xu, X., Ren, W., Pan, S., & Chappelka, A. (2010). Model estimates of net primary productivity, evapotranspiration, and water use efficiency in the terrestrial ecosystems of the southern United States during 1895–2007. *Forest ecology and management*, 259(7), 1311–1327. <https://doi.org/10.1016/j.foreco.2009.10.009>
44. Wu, J., Roulet, N. T., Sagerfors, J., & Nilsson, M. B. (2013). Simulation of six years of carbon fluxes for a sedge-dominated oligotrophic minerogenic peatland in Northern Sweden using the McGill Wetland Model (MWM). *Journal of Geophysical Research: Biogeosciences*, 118(2), 795–807. <https://doi.org/10.1002/jgrg.20045>
45. Ju, W., Gao, P., Zhou, Y., Chen, J. M., Chen, S., & Li, X. (2010). Prediction of summer grain crop yield with a process-based ecosystem model and remote sensing data for the northern area of the Jiangsu Province. *China. International Journal of Remote Sensing*, 31(6), 1573–1587. <https://doi.org/10.1080/01431160903475357>
46. Mariani, L. (2017). Carbon plants nutrition and global food security. *The European Physical Journal Plus*, 132(2), 1–14. <https://doi.org/10.1140/epjp/i2017-11337-8>
47. Yao, F., Tang, Y., Wang, P., & Zhang, J. (2015). Estimation of maize yield by using a process-based model and remote sensing data in the Northeast China Plain. *Physics and Chemistry of the Earth, Parts A/B/C*, 87, 142–152. <https://doi.org/10.1016/j.pce.2015.08.010>
48. Chipanshi, A., Zhang, Y., Kouadio, L., Newlands, N., Davidson, A., Hill, H., Warren, R., Qian, B., Daneshfar, B., Bedard, F., & Reichert, G. (2015). Evaluation of the Integrated Canadian Crop Yield Forecaster (ICCYF) model for in-season prediction of crop yield across the Canadian agricultural landscape. *Agricultural and Forest Meteorology*, 206, 137–150. <https://doi.org/10.1016/j.agrformet.2015.03.007>
49. Zwart, S. J., Bastiaanssen, W. G., de Fraiture, C., & Molden, D. J. (2010). WATPRO: A remote sensing based model for mapping water productivity of wheat. *Agricultural Water Management*, 97(10), 1628–1636. <https://doi.org/10.1016/j.agwat.2010.05.017>
50. Abedinpour, M., Sarangi, A., Rajput, T. B. S., Singh, M., Pathak, H., & Ahmad, T. (2012). Performance evaluation of AquaCrop model for maize crop in a semi-arid environment. *Agricultural Water Management*, 110, 55–66. <https://doi.org/10.1016/j.agwat.2012.04.001>
51. Ines, A. V., Das, N. N., Hansen, J. W., & Njoku, E. G. (2013). Assimilation of remotely sensed soil moisture and vegetation with a crop simulation model for maize yield prediction. *Remote Sensing of Environment*, 138, 149–164. <https://doi.org/10.1016/j.rse.2013.07.018>
52. Kumar, P., Sarangi, A., Singh, D. K., Parihar, S. S., & Sahoo, R. N. (2015). Simulation of salt dynamics in the root zone and yield of wheat crop under irrigated saline regimes using SWAP model. *Agricultural Water Management*, 148, 72–83. <https://doi.org/10.1016/j.agwat.2014.09.014>
53. Lobell, D. B., & Burke, M. B. (2010). On the use of statistical models to predict crop yield responses to climate change. *Agricultural and forest meteorology*, 150(11), 1443–1452. <https://doi.org/10.1016/j.agrformet.2010.07.008>
54. Lobell, D. B., Thau, D., Seifert, C., Engle, E., & Little, B. (2015). A scalable satellite-based crop yield mapper. *Remote Sensing of Environment*, 164, 324–333. <https://doi.org/10.1016/j.rse.2015.04.021>
55. Sibley, A. M., Grassini, P., Thomas, N. E., Cassman, K. G., & Lobell, D. B. (2014). Testing remote sensing approaches for assessing yield variability among maize fields. *Agronomy Journal*, 106(1), 24–32. <https://doi.org/10.2134/agronj2013.0314>
56. Newlands, N. K., Zamar, D. S., Kouadio, L. A., Zhang, Y., Chipanshi, A., Potgieter, A., Toure, S., & Hill, H. S. (2014). An integrated, probabilistic model for improved seasonal forecasting of agricultural crop yield under environmental uncertainty. *Frontiers in Environmental Science*, 2, 17. <https://doi.org/10.3389/fenvs.2014.00017>
57. Choudhury, A., & Jones, J. (2014). Crop yield prediction using time series models. *Journal of Economics and Economic Education Research*, 15(3), 53.
58. Suresh, K. K., & Priya, S. K. (2011). Forecasting sugarcane yield of Tamil Nadu using ARIMA models. *Sugar Tech*, 13(1), 23–26. <https://doi.org/10.1007/s12355-011-0071-7>
59. Yildirak, K., Kalaylioglu, Z., & Mermer, A. (2015). Bayesian estimation of crop yield function: Drought based wheat prediction model for tigem farms. *Environmental and ecological statistics*, 22(4), 693–704. <https://doi.org/10.1007/s10651-015-0327-6>
60. You, J., Li, X., Low, M., Lobell, D., & Ermon, S. (2017). Deep Gaussian process for crop yield prediction based on remote sensing data. In *Proceedings of the AAAI Conference on Artificial Intelligence*, 31(1).
61. Boote, K. J., Jones, J. W., & Pickering, N. B. (1996). Potential uses and limitations of crop models. *Agronomy journal*, 88(5), 704–716. <https://doi.org/10.2134/agronj1996.00021962008800050005x>
62. Chenu, K., Porter, J. R., Martre, P., Basso, B., Chapman, S. C., Ewert, F., Bindi, M., & Asseng, S. (2017). Contribution of crop models to adaptation in wheat. *Trends in plant science*, 22(6), 472–490. <https://doi.org/10.1016/j.tplants.2017.02.003>
63. Anagnostopoulos, V., Petropoulos, G. P., Ireland, G., & Carlson, T. N. (2017). A modernized version of a 1D soil vegetation atmosphere transfer model for improving its future use in land surface interactions studies. *Environmental Modelling & Software*, 90, 147–156. <https://doi.org/10.1016/j.envsoft.2017.01.004>
64. Arnold, J.G., Moriasi, D.N., Gassman, P.W., Abbaspour, K.C., White, M.J., Srinivasan, R., Santhi, C., Harmel, R.D., Van Griensven, A., Van Liew, M.W. & Kannan, N. (2012). SWAT: Model use, calibration, and validation. *Transactions of the ASABE*, 55(4), 1491–1508. <https://doi.org/10.13031/2013.42256>
65. Ferrant, S., Oehler, F., Durand, P., Ruiz, L., Salmon-Monviola, J., Justes, E., Dugast, P., Probst, A., Probst, J. L., & Sanchez-Perez, J. M. (2011). Understanding nitrogen transfer dynamics in a small agricultural catchment: Comparison of a distributed (TNT2) and a semi distributed (SWAT) modeling approaches. *Journal of hydrology*, 406(1–2), 1–15. <https://doi.org/10.1016/j.jhydrol.2011.05.026>
66. Castañeda-Vera, A., Leffelaar, P. A., Álvaro-Fuentes, J., Cantero-Martínez, C., & Mínguez, M. I. (2015). Selecting crop models for decision making in wheat insurance. *European Journal of Agronomy*, 68, 97–116. <https://doi.org/10.1016/j.eja.2015.04.008>
67. Li, T., Hasegawa, T., Yin, X., Zhu, Y., Boote, K., Adam, M., Bregaglio, S., Buis, S., Confalonieri, R., Fumoto, T., & Gaydon, D. (2015). Uncertainties in predicting rice yield by current crop models under a wide range of climatic conditions. *Global change biology*, 21(3), 1328–1341. <https://doi.org/10.1111/gcb.12758>
68. Steduto, P., Hsiao, T. C., Raes, D., & Fereres, E. (2009). AquaCrop—The FAO crop model to simulate yield response to water: I. Concepts and underlying principles. *Agronomy Journal*, 101(3), 426–437. <https://doi.org/10.2134/agronj2008.0139s>
69. van Ittersum, M. K., Leffelaar, P. A., van Keulen, H., Kropff, M. J., Bastiaans, L., & Goudriaan, J. (2003). On approaches and applications of the Wageningen crop models. *European*

- journal of agronomy*, 18(3–4), 201–234. [https://doi.org/10.1016/S1161-0301\(02\)00106-5](https://doi.org/10.1016/S1161-0301(02)00106-5)
70. Rosenzweig, C., Elliott, J., Deryng, D., Ruane, A. C., Müller, C., Arneth, A., Boote, K. J., Folberth, C., Glotter, M., Khabarov, N., & Neumann, K. (2014). Assessing agricultural risks of climate change in the 21st century in a global gridded crop model inter-comparison. *Proceedings of the National Academy of Sciences*, 111(9), 3268–3273. <https://doi.org/10.1073/pnas.1222463110>
 71. McMaster, G. S., White, J. W., Hunt, L. A., Jamieson, P. D., Dhillon, S. S., & Ortiz-Monasterio, J. I. (2008). Simulating the influence of vernalization, photoperiod and optimum temperature on wheat developmental rates. *Annals of botany*, 102(4), 561–569. <https://doi.org/10.1093/aob/mcn115>
 72. Yin, X., Kropff, M. J., McLaren, G., & Visperas, R. M. (1995). A nonlinear model for crop development as a function of temperature. *Agricultural and Forest Meteorology*, 77(1–2), 1–16. [https://doi.org/10.1016/0168-1923\(95\)02236-Q](https://doi.org/10.1016/0168-1923(95)02236-Q)
 73. De Wit, C.T. (1978). Simulation of assimilation, respiration and transpiration of crops.
 74. Farquhar, G. D., von Caemmerer, S. V., & Berry, J. A. (1980). A biochemical model of photosynthetic CO₂ assimilation in leaves of C₃ species. *Planta*, 149(1), 78–90. <https://doi.org/10.1007/BF00386231>
 75. He, D., Wang, E., Wang, J., & Robertson, M. J. (2017). Data requirement for effective calibration of process-based crop models. *Agricultural and forest meteorology*, 234, 136–148. <https://doi.org/10.1016/j.agrformet.2016.12.015>
 76. Wallach, D., Makowski, D., Jones, J. W., & Brun, F. (2006). *Working with dynamic crop models: Evaluation, analysis, parameterization, and applications*. Elsevier.
 77. Parent, B., & Tardieu, F. (2014). Can current crop models be used in the phenotyping era for predicting the genetic variability of yield of plants subjected to drought or high temperature? *Journal of experimental botany*, 65(21), 6179–6189. <https://doi.org/10.1093/jxb/eru223>
 78. Horie, T., Nakagawa, H., Centeno, H.G.S. & Kropff, M.J. (1995). The rice crop simulation model SIMRIW and its testing. *Modeling the impact of climate change on rice production in Asia*, 51–66.
 79. Nguyen, D. N., Lee, K. J., Kim, D. I., Anh, N. T., & Lee, B. W. (2014). Modeling and validation of high-temperature induced spikelet sterility in rice. *Field crops research*, 156, 293–302. <https://doi.org/10.1016/j.fcr.2013.11.009>
 80. Durand, J. L., Delusca, K., Boote, K., Lizaso, J., Manderscheid, R., Weigel, H. J., Ruane, A. C., Rosenzweig, C., Jones, J., Ahuja, L., & Anapalli, S. (2018). How accurately do maize crop models simulate the interactions of atmospheric CO₂ concentration levels with limited water supply on water use and yield? *European journal of agronomy*, 100, 67–75. <https://doi.org/10.1016/j.eja.2017.01.002>
 81. Engineer, C. B., Hashimoto-Sugimoto, M., Negi, J., Israelsson-Nordström, M., Azoulay-Shemer, T., Rappel, W. J., Iba, K., & Schroeder, J. I. (2016). CO₂ sensing and CO₂ regulation of stomatal conductance: Advances and open questions. *Trends in Plant Science*, 21(1), 16–30. <https://doi.org/10.1016/j.tplants.2015.08.014>
 82. Vanuytrecht, E., & Thorburn, P. J. (2017). Responses to atmospheric CO₂ concentrations in crop simulation models: A review of current simple and semicomplex representations and options for model development. *Global change biology*, 23(5), 1806–1820. <https://doi.org/10.1111/gcb.13600>
 83. Blanc, É. (2017). Statistical emulators of maize, rice, soybean and wheat yields from global gridded crop models. *Agricultural and Forest Meteorology*, 236, 145–161. <https://doi.org/10.1016/j.agrformet.2016.12.022>
 84. Liu, J., Williams, J. R., Zehnder, A. J., & Yang, H. (2007). GEPIC—modelling wheat yield and crop water productivity with high resolution on a global scale. *Agricultural systems*, 94(2), 478–493. <https://doi.org/10.1016/j.agsy.2006.11.019>
 85. Ashraf Vaghefi, S., Abbaspour, K. C., Faramarzi, M., Srinivasan, R., & Arnold, J. G. (2017). Modeling crop water productivity using a coupled SWAT–MODSIM model. *Water*, 9(3), 157. <https://doi.org/10.3390/w9030157>
 86. Srinivasan, R., Zhang, X., & Arnold, J. (2010). SWAT ungauged: Hydrological budget and crop yield predictions in the Upper Mississippi River Basin. *Transactions of the ASABE*, 53(5), 1533–1546. <https://doi.org/10.13031/2013.34903>
 87. Yang, Q., Zhang, X., Almendinger, J. E., Huang, M., Leng, G., Zhou, Y., Zhao, K., Asrar, G. R., Li, X., & Qiu, J. (2019). Improving the SWAT forest module for enhancing water resource projections: A case study in the St. Croix River basin. *Hydrological Processes*, 33(5), 864–875. <https://doi.org/10.1002/hyp.13370>
 88. Wang, E., Martre, P., Zhao, Z., Ewert, F., Maiorano, A., Rötter, R. P., Kimball, B. A., Ottman, M. J., Wall, G. W., White, J. W., & Reynolds, M. P. (2017). The uncertainty of crop yield projections is reduced by improved temperature response functions. *Nature plants*, 3(8), 1–13. <https://doi.org/10.1038/nplants.2017.102>
 89. Wagle, P., Zhang, Y., Jin, C., & Xiao, X. (2016). Comparison of solar-induced chlorophyll fluorescence, light-use efficiency, and process-based GPP models in maize. *Ecological Applications*, 26(4), 1211–1222. <https://doi.org/10.1890/15-1434>
 90. Zhang, L. X., Zhou, D. C., Fan, J. W., & Hu, Z. M. (2015). Comparison of four light use efficiency models for estimating terrestrial gross primary production. *Ecological Modelling*, 300, 30–39. <https://doi.org/10.1016/j.ecolmodel.2015.01.001>
 91. He, M., Ju, W., Zhou, Y., Chen, J., He, H., Wang, S., Wang, H., Guan, D., Yan, J., Li, Y., & Hao, Y. (2013). Development of a two-leaf light use efficiency model for improving the calculation of terrestrial gross primary productivity. *Agricultural and forest meteorology*, 173, 28–39. <https://doi.org/10.1016/j.agrformet.2013.01.003>
 92. Zhou, Y., Wu, X., Ju, W., Chen, J. M., Wang, S., Wang, H., Yuan, W., Andrew Black, T., Jassal, R., Ibrom, A., & Han, S. (2016). Global parameterization and validation of a two-leaf light use efficiency model for predicting gross primary production across FLUXNET sites. *Journal of Geophysical Research: Biogeosciences*, 121(4), 1045–1072. <https://doi.org/10.1002/2014JG002876>
 93. McCallum, I., Franklin, O., Moltchanova, E., Merbold, L., Schullius, C., Shvidenko, A., Schepaschenko, D., & Fritz, S. (2013). Improved light and temperature responses for light-use-efficiency-based GPP models. *Biogeosciences*, 10(10), 6577–6590. <https://doi.org/10.5194/bg-10-6577-2013>
 94. Wei, S., Yi, C., Fang, W., & Hendrey, G. (2017). A global study of GPP focusing on light-use efficiency in a random forest regression model. *Ecosphere*, 8(5), e01724. <https://doi.org/10.1002/ecs2.1724>
 95. Yuan, W., Cai, W., Xia, J., Chen, J., Liu, S., Dong, W., Merbold, L., Law, B., Arain, A., Beringer, J., & Bernhofer, C. (2014). Global comparison of light use efficiency models for simulating terrestrial vegetation gross primary production based on the LaThuile database. *Agricultural and Forest Meteorology*, 192, 108–120. <https://doi.org/10.1016/j.agrformet.2014.03.007>
 96. Bandaru, V., West, T. O., Ricciuto, D. M., & Izaurralde, R. C. (2013). Estimating crop net primary production using national inventory data and MODIS-derived parameters. *ISPRS Journal of Photogrammetry and Remote Sensing*, 80, 61–71. <https://doi.org/10.1016/j.isprsjprs.2013.03.005>
 97. Jin, N., Ren, W., Tao, B., He, L., Ren, Q., Li, S., & Yu, Q. (2018). Effects of water stress on water use efficiency of irrigated and rainfed wheat in the Loess Plateau, China. *Science of the total environment*, 642, 1–11. <https://doi.org/10.1016/j.scitotenv.2018.06.028>
 98. Tao, F., Yokozawa, M., Zhang, Z., Xu, Y., & Hayashi, Y. (2005). Remote sensing of crop production in China by production efficiency models: Models comparisons, estimates and uncertainties.

- Ecological modelling*, 183(4), 385–396. <https://doi.org/10.1016/j.ecolmodel.2004.08.023>
99. Rahman, M. M., Lamb, D. W., Stanley, J. N., & Trotter, M. G. (2014). Use of proximal sensors to evaluate at the sub-paddock scale a pasture growth-rate model based on light-use efficiency. *Crop and Pasture Science*, 65(4), 400–409. <https://doi.org/10.1071/CP14071>
 100. Potter, C. S., Randerson, J. T., Field, C. B., Matson, P. A., Vitousek, P. M., Mooney, H. A., & Klooster, S. A. (1993). Terrestrial ecosystem production: A process model based on global satellite and surface data. *Global Biogeochemical Cycles*, 7(4), 811–841. <https://doi.org/10.1029/93GB02725>
 101. Running, S.W., Nemani, R., Glassy, J.M. & Thornton, P.E. (1999b). MODIS daily photosynthesis (PSN) and annual net primary production (NPP) product (MOD17) Algorithm Theoretical Basis Document. University of Montana, SCF At-Launch Algorithm ATBD Documents (available online at: www.ntsg.umt.edu/modis/ATBD/ATBD_MOD17_v21.pdf), 490.
 102. Running, S.W. & Zhao, M. (2015). Daily GPP and annual NPP (MOD17A2/A3) products NASA Earth Observing System MODIS land algorithm. *MOD17 User's Guide*, 2015, 1–28.
 103. Running, S. W., Myneni, R. B., Nemani, R. R., & Glassy, J. (1996). *MOD15 LAI/FPAR Algorithm Theoretical Basis Document*. NASA Headquarters.
 104. Doughty, R., Kurosu, T.P., Parazoo, N., Köhler, P., Wang, Y., Sun, Y. & Frankenberg, C. (2022). Global GOSAT, OCO-2, and OCO-3 solar-induced chlorophyll fluorescence datasets. *Earth System Science Data*, 14(4), 1513–1529. <https://doi.org/10.5194/essd-2021-237>.
 105. Brown, L.A., Dash, J., Lidón, A.L., Lopez-Baeza, E. & Dransfeld, S. (2019). Synergetic exploitation of the Sentinel-2 missions for validating the Sentinel-3 ocean and land color instrument terrestrial chlorophyll index over a vineyard dominated Mediterranean environment. *IEEE Journal of Selected Topics in Applied Earth Observations and Remote Sensing*, 12(7), 2244–2251. <https://doi.org/10.1109/JSTARS.2019.2899998>
 106. Gentine, P., & Alemohammad, S. H. (2018). Reconstructed solar-induced fluorescence: A machine learning vegetation product based on MODIS surface reflectance to reproduce GOME-2 solar-induced fluorescence. *Geophysical research letters*, 45(7), 3136–3146. <https://doi.org/10.1002/2017GL076294>
 107. Sun, Y., Frankenberg, C., Jung, M., Joiner, J., Guanter, L., Köhler, P., & Magney, T. (2018). Overview of solar-induced chlorophyll fluorescence (SIF) from the Orbiting Carbon Observatory-2: Retrieval, cross-mission comparison, and global monitoring for GPP. *Remote Sensing of Environment*, 209, 808–823. <https://doi.org/10.1016/j.rse.2018.02.016>
 108. Vuolo, F., Dash, J., Curran, P. J., Lajas, D., & Kwiatkowska, E. (2012). Methodologies and uncertainties in the use of the terrestrial chlorophyll index for the sentinel-3 mission. *Remote Sensing*, 4(5), 1112–1133. <https://doi.org/10.3390/rs4051112>
 109. Haxeltine, A. & Prentice, I.C. (1996). A general model for the light-use efficiency of primary production. *Functional Ecology*, 551–561. <https://doi.org/10.2307/2390165>
 110. He, L., Magney, T., Dutta, D., Yin, Y., Köhler, P., Grossmann, K., Stutz, J., Dold, C., Hatfield, J., Guan, K. & Peng, B. (2020). From the ground to space: Using solar-induced chlorophyll fluorescence to estimate crop productivity. *Geophysical Research Letters*, 47(7), e2020GL087474. <https://doi.org/10.1029/2020GL087474>
 111. Wang, C., Guan, K., Peng, B., Chen, M., Jiang, C., Zeng, Y., Wu, G., Wang, S., Wu, J., Yang, X. & Frankenberg, C. (2020). Satellite footprint data from OCO-2 and TROPOMI reveal significant spatio-temporal and inter-vegetation type variabilities of solar-induced fluorescence yield in the US Midwest. *Remote Sensing of Environment*, 241, 111728. <https://doi.org/10.1016/j.rse.2020.111728>
 112. Wang, S., Zhang, Y., Ju, W., Wu, M., Liu, L., He, W., & Peñuelas, J. (2022). Temporally corrected long-term satellite solar-induced fluorescence leads to improved estimation of global trends in vegetation photosynthesis during 1995–2018. *ISPRS Journal of Photogrammetry and Remote Sensing*, 194, 222–234. <https://doi.org/10.1016/j.isprsjprs.2022.10.018>
 113. Wang, Q., Shi, W., Atkinson, P. M., & Zhao, Y. (2015). Downscaling MODIS images with area-to-point regression kriging. *Remote Sensing of Environment*, 166, 191–204. <https://doi.org/10.1016/j.rse.2015.06.003>
 114. Stathopoulou, M., & Cartalis, C. (2009). Downscaling AVHRR land surface temperatures for improved surface urban heat island intensity estimation. *Remote Sensing of Environment*, 113(12), 2592–2605. <https://doi.org/10.1016/j.rse.2009.07.017>
 115. Price, J. C. (1987). Combining panchromatic and multispectral imagery from dual resolution satellite instruments. *Remote sensing of environment*, 21(2), 119–128. [https://doi.org/10.1016/0034-4257\(87\)90049-6](https://doi.org/10.1016/0034-4257(87)90049-6)
 116. Gelfand, A. E., Zhu, L., & Carlin, B. P. (2001). On the change of support problem for spatio-temporal data. *Biostatistics*, 2(1), 31–45. <https://doi.org/10.1093/biostatistics/2.1.31>
 117. Carlin, B.P., Xia, H., Devine, O., Tolbert, P. & Mulholland, J. (1999). Spatio-temporal hierarchical models for analyzing Atlanta pediatric asthma ER visit rates. *In Case studies in Bayesian statistics*, 303–320. Springer, New York, NY.
 118. Kyriakidis, P. C. (2004). A geostatistical framework for area-to-point spatial interpolation. *Geographical Analysis*, 36(3), 259–289. <https://doi.org/10.1111/j.1538-4632.2004.tb01135.x>
 119. Kyriakidis, P. C., & Yoo, E. H. (2005). Geostatistical prediction and simulation of point values from areal data. *Geographical Analysis*, 37(2), 124–151. <https://doi.org/10.1111/j.1538-4632.2005.00633.x>
 120. Atkinson, P. M. (2013). Downscaling in remote sensing. *International Journal of Applied Earth Observation and Geoinformation*, 22, 106–114. <https://doi.org/10.1016/j.jag.2012.04.012>
 121. Atkinson, P. M. (1997). Mapping sub-pixel boundaries from remotely sensed images. *Innovations in GIS*, 4, 166–180.
 122. Atkinson, P. M., Pardo-Iguzquiza, E., & Chica-Olmo, M. (2008). Downscaling cokriging for super-resolution mapping of continua in remotely sensed images. *IEEE Transactions on Geoscience and Remote Sensing*, 46(2), 573–580. <https://doi.org/10.1109/TGRS.2007.909952>
 123. Nguyen, M. Q., Atkinson, P. M., & Lewis, H. G. (2006). Super-resolution mapping using a Hopfield neural network with fused images. *IEEE Transactions on Geoscience and Remote Sensing*, 44(3), 736–749. <https://doi.org/10.1109/TGRS.2005.861752>
 124. Nguyen, Q. M., Atkinson, P. M., & Lewis, H. G. (2011). Super-resolution mapping using Hopfield neural network with panchromatic imagery. *International journal of remote sensing*, 32(21), 6149–6176. <https://doi.org/10.1080/01431161.2010.507797>
 125. Chen, Y., Ge, Y., An, R., & Chen, Y. (2018). Super-resolution mapping of impervious surfaces from remotely sensed imagery with points-of-interest. *Remote Sensing*, 10(2), 242. <https://doi.org/10.3390/rs10020242>
 126. Ling, F., & Foody, G. M. (2019). Super-resolution land cover mapping by deep learning. *Remote Sensing Letters*, 10(6), 598–606. <https://doi.org/10.1080/2150704X.2019.1587196>
 127. Ling, F., Zhang, Y., Foody, G.M., Li, X., Zhang, X., Fang, S., Li, W. & Du, Y. (2016). Learning-based superresolution land cover mapping. *IEEE Transactions on Geoscience and Remote Sensing*, 54(7), 3794–3810. <https://doi.org/10.1109/TGRS.2016.2527841>
 128. Muad, A.M. & Foody, G.M. (2012). Impact of land cover patch size on the accuracy of patch area representation in HNN-based super resolution mapping. *IEEE Journal of Selected Topics in Applied Earth Observations and Remote Sensing*, 5(5), 1418–1427. <https://doi.org/10.1109/JSTARS.2012.2191145>

129. Kim, J., Lee, J.K. & Lee, K.M. (2016). Accurate image super-resolution using very deep convolutional networks. *In Proceedings of the IEEE conference on computer vision and pattern recognition*, 1646–1654.
130. Duveiller, G., & Cescatti, A. (2016). Spatially downscaling sun-induced chlorophyll fluorescence leads to an improved temporal correlation with gross primary productivity. *Remote Sensing of Environment*, 182, 72–89. <https://doi.org/10.1016/j.rse.2016.04.027>
131. Wen, J., Köhler, P., Duveiller, G., Parazoo, N.C., Magney, T.S., Hooker, G., Yu, L., Chang, C.Y. & Sun, Y. (2020). A framework for harmonizing multiple satellite instruments to generate a long-term global high spatial-resolution solar-induced chlorophyll fluorescence (SIF). *Remote Sensing of Environment*, 239, 111644. <https://doi.org/10.1016/j.rse.2020.111644>
132. Basso, B., Cammarano, D. & Carfagna, E. (2013). Review of crop yield forecasting methods and early warning systems. *In Proceedings of the first meeting of the scientific advisory committee of the global strategy to improve agricultural and rural statistics, FAO Headquarters, Rome, Italy*, 241.
133. Cammarano, D. (2009). Spatial integration of remote sensing and crop simulation modelling for wheat nitrogen management (Doctoral dissertation, University of Melbourne, Melbourne School of Land and Environment, Department of Resource Management and Geography).
134. de Wit, A.J.W. (2007). Regional crop yield forecasting using probabilistic crop growth modelling and remote sensing data assimilation.
135. Prasad, A. K., Chai, L., Singh, R. P., & Kafatos, M. (2006). Crop yield estimation model for Iowa using remote sensing and surface parameters. *International Journal of Applied earth observation and geoinformation*, 8(1), 26–33.
136. Schut, A. G. T., Stephens, D. J., Stovold, R. G. H., Adams, M., & Craig, R. L. (2009). Improved wheat yield and production forecasting with a moisture stress index, AVHRR and MODIS data. *Crop and Pasture Science*, 60(1), 60–70. <https://doi.org/10.1071/CP08182>
137. Kuwata, K., & Shibasaki, R. (2015, July). Estimating crop yields with deep learning and remotely sensed data. In *2015 IEEE International Geoscience and Remote Sensing Symposium (IGARSS)* (pp. 858–861). IEEE. <https://doi.org/10.1109/IGARSS.2015.7325900>
138. Sabzchi-Dehkharghani, H., Nazemi, A.H., Sadraddini, A.A., Majnooni-Heris, A. & Biswas, A. (2021). Recognition of different yield potentials among rain-fed wheat fields before harvest using remote sensing. *Agricultural Water Management*, 245, 106611. <https://doi.org/10.1016/j.agwat.2020.106611>
139. Liu, Y., Chen, J.M., He, L., Zhang, Z., Wang, R., Rogers, C., Fan, W., de Oliveira, G. & Xie, X. (2022). Non-linearity between gross primary productivity and far-red solar-induced chlorophyll fluorescence emitted from canopies of major biomes. *Remote Sensing of Environment*, 271, 112896. <https://doi.org/10.1016/j.rse.2022.112896>
140. Halubok, M., & Yang, Z. L. (2020). Estimating crop and grass productivity over the United States using satellite solar-induced chlorophyll fluorescence, precipitation and soil moisture data. *Remote Sensing*, 12(20), 3434. <https://doi.org/10.3390/rs12203434>
141. Tagesson, T., Ardö, J., Cappelaere, B., Kergoat, L., Abdi, A., Horion, S., & Fensholt, R. (2017). Modelling spatial and temporal dynamics of gross primary production in the Sahel from earth-observation-based photosynthetic capacity and quantum efficiency. *Biogeosciences*, 14(5), 1333–1348. <https://doi.org/10.5194/bg-14-1333-2017>

Publisher's Note Springer Nature remains neutral with regard to jurisdictional claims in published maps and institutional affiliations.

Springer Nature or its licensor (e.g. a society or other partner) holds exclusive rights to this article under a publishing agreement with the author(s) or other rightsholder(s); author self-archiving of the accepted manuscript version of this article is solely governed by the terms of such publishing agreement and applicable law.